SATELLITE-TRACKING AND EARTH-DYNAMICS RESEARCH PROGRAMS

Grant Number NGR 09-015-002

Semiannual Progress Report No. 32

1 January to 30 June 1975

Project Director: Dr. G. C. Weiffenbach

Prepared for

National Aeronautics and Space Administration
Washington, D.C. 20546

Smithsonian Institution
Astrophysical Observatory
Cambridge, Massachusetts 02138

The Smithsonian Astrophysical Observatory
and the Harvard College Observatory
are members of the
Center for Astrophysics

SATELLITE-TRACKING AND EARTH-DYNAMICS RESEARCH PROGRAMS

Grant Number NGR 09-015-002

Semiannual Progress Report No. 32

1 January to 30 June 1975

Project Director: Dr. G. C. Weiffenbach

Prepared for

National Aeronautics and Space Administration
Washington, D.C. 20546

Smithsonian Institution
Astrophysical Observatory
Cambridge, Massachusetts 02138

The Smithsonian Astrophysical Observatory
and the Harvard College Observatory
are members of the
Center for Astrophysics

TABLE OF CONTENTS

TABLE OF CONTENTS (Cont.)

SATELLITE-TRACKING AND EARTH-DYNAMICS RESEARCH PROGRAMS

Semiannual Progress Report No. 32

1. INTRODUCTION

This report describes the activities and progress in the satellite-tracking and earth-dynamics research programs during the first half of calendar year 1975. It is divided into five sections, this introduction including some of the highlights of the period. Section 2 is devoted to satellite-tracking network operations. Section 3 covers satellite geodesy and geophysics programs. Geos 3 project support is addressed in Section 4, while atmospheric research is described in Section 5.

The major thrust in the satellite-tracking area continues to be improved accuracy in laser ranging. Coupled with this is the use of automated, field-generated predictions, which increased the quantity of data and should effect cost savings through reduced communications and computer usage.

During this report period, the Smithsonian Astrophysical Observatory (SAO) network of observing stations obtained over 88,600 laser returns from the Geos 1, Geos 2, Geos 3, BE-C, and Starlette satellites. This is the largest amount of data ever acquired over a comparable period of time and is nearly three times that of the same period last year. New records have also been set in total-network and individual-station performance. The data increase is a reflection of both the increased laser pulse-repetition rate and the intensive tracking effort in support of the Geos 3 observation campaign, which is centered around the recently launched Geos 3 and Starlette satellites.

Progress continues in all areas of the laser-upgrading program. In January, the prototype version of the pulse-processing system at Mt. Hopkins,

Arizona, was modified to the production version, and it has been operational since that time. Other systems are on site or in transit; they will be installed during local poor-weather periods to provide minimum interference with the Geos 3 observation schedule. The system originally destined for South Africa will be installed after the station has been moved to Australia.

Both the 8-pulse-per-minute modification and the field minicomputer systems have been installed and are operational at all stations. The four SAO laser stations now generate their own laser predictions from orbital elements furnished by Cambridge. Factory acceptance testing was conducted on the first pulse-chopper modification to the laser system, and design changes are in progress at the manufacturer.

Within the geodesy and geophysics programs, work continues on deriving a more detailed and more accurate model of the gravity field. Computer programs have been rewritten that yield substantial improvements in this area. As a result, for example, more coefficients can be calculated from surface-gravity data. The number of 1° X 1° measured means of surface-gravity data and the number of calculated 550-km X 550-km block anomalies with total coverage have both increased significantly (by 78 and 24%, respectively) since publication of the 1973 Smithsonian Standard Earth (III) (SE III) (Gaposchkin, 1973).

Analytical formulas of gravitational perturbations are being revised to achieve higher accuracy in orbit determination and ephemeris computation. Complete third-order expressions for zonal-harmonics perturbations are being developed in terms of both Hill and Delaunay variables by use of computer algebra.

Of major concern in obtaining more precise data from the tracking of satellites is the selection of future observing sites. A geological and geophysical investigation of 26 existing or proposed laser-station locations is now nearly completed.

Final data from the ESRO 4 gas analyzer have been received and studied. The upper atmospheric research group has been analyzing these data to construct a global model of the atmospheric variations that accompany geomagnetic disturbances.

2. SATELLITE-TRACKING NETWORK OPERATIONS

2.1 Satellite Observing Campaigns

The SAO network tracked the Geos 1, Geos 2, Geos 3, BE-C, and Starlette satellites to provide data for its on-going research program in geophysics supported by the National Aeronautics and Space Administration (NASA).

Starlette was launched on 6 February 1975; as soon as an accurate orbit was established, it was included in SAO's complement of routinely tracked laser satellites. Because of its 50° inclination, unique among the laser satellites, Starlette will make a particularly important contribution to the next SAO-determined gravity-field solution.

With its launch on 9 April 1975, Geos 3 initiated the most extensive international satellite-tracking campaign organized to date. This satellite is being tracked intensively by the laser (and Baker-Nunn camera) systems of SAO's station network and by tracking instrumentation belonging to other organizations throughout the world. SAO has coordinated the international tracking campaign, and the SAO laser network has been observing Geos 3 at highest priority since launch.

2.2 Laser Data

Statistics for the period January through June 1975 for the SAO laser stations in Arizona, Brazil, Peru, and South Africa represent the largest number of data points ever recorded over any comparable period of time. The SAO network acquired 88,608 points on 2248 satellite arcs (see Table 1), or nearly 3 times the number of range measurements recorded during the same period last year.

New records were established for overall-network and individual-station performance at each of the SAO laser stations during this report period. All

Table 1. Successful laser measurements (numbers in parentheses are successful arcs).

Month	South Africa		Peru		Mt. Hopkins		Brazil		Total SAO	
January	1339	(44)	1005	(52)	2455	(71)	2628	(130)	7427	(297)
February	437	(23)	191	(15)	4348	(80)	2473	(67)	7449	(185)
March	598	(31)	812	(47)	1602	(27)	2336	(67)	5348	(172)
April	2094	(90)	6608	(182)	*		5888	(141)	14590	(413)
May	7322	(150)	10968	(225)	2037	(43)*	2819	(94)	23146	(512)
June	10797	(217)	11345	(249)	5668	(105)	2838	(98)	30648	(669)
Total	22587	(555)	30929	(770)	16110	(326)	18982	(597)	88608	(2248)

Cooperating Stations, January to June 1975

Grand Canary Islands	97	(11)
Grasse	177	(19)
Greece	1478	(231)
Japan	197	(20)
Wettzell	167	(20)

* Data taken during this period with the new pulse processor are being analyzed now.

stations set records in numbers of points, and Brazil and South Africa, in numbers of arcs. Peru holds the single-station network record with 11,345 points, acquired during June. A total-network record in numbers of points and numbers of arcs was also established in June, with 30,648 points on 669 satellite passes. This number of points, for the month of June alone, is nearly equal to the total number of points for the first 6 months of CY 1974.

The large number of range measurements acquired from January to June is a reflection both of the newly implemented 8-pulse-per-minute laser modification (see Section 2.4) and of the increased number of satellites being tracked under the Geos 3 observation program.

The Tokyo Astronomical Observatory (TAO) operated its laser system through April, acquiring 197 data points on 20 satellite arcs. The system ceased operation at that time because of weather conditions and equipment refurbishment.

The laser system in Dionysos, Greece, owned by our cooperating agency, the National Technical University (NTU) of Athens, continued routine operations; 1478 range measurements were taken on 231 satellite passes.

The French Office National d'Études et de Recherches Aérospatiales and Centre National d'Études Spatiales (CNES) operated laser systems at Grasse, France, and the Grand Canary Islands. These systems acquired 177 and 97 points on 19 and 11 satellite arcs, respectively. In addition, the Federal Republic of Germany laser at Wettzell, Germany, acquired 167 points on 20 satellite passes. The French and German lasers contributed these data in support of the Geos 3 observation program.

2.3 Baker-Nunn Cameras

Ten Baker-Nunn cameras operated by SAO and its cooperating agencies obtained over 6200 successful observations of 18 satellites (see Table 2). These routine observations are used primarily to generate pointing predictions for the laser systems. The Baker-Nunn network provided slightly over 1800

successful observations on five atmospheric satellites in support of NASA-sponsored research conducted by Dr. L. G. Jacchia (see Table 3).

The French Groupe de Recherches de Geodésie Spatiale launched the D5B satellite on 17 May 1975. Although this spacecraft is equipped with laser corner cubes, SAO tracks it with the Baker-Nunn camera systems only. Its low orbit makes it difficult to acquire with laser systems, and it is not being used for SAO or NASA geophysical research.

The first Indian artificial earth satellite was launched on 19 April 1975. This object was designed to be in orbit for 6 months to study x-radiation and gamma radiation and to measure the outer layers of the earth's atmosphere. The SAO Baker-Nunn network is tracking it under special request from the Indian National Space Agency and will continue to do so for the 6-month experiment period, although the satellite is difficult to acquire because of its low orbit and small size.

Tracking support continued on satellite 1971 54A for Dr. D. King-Hele of the British Royal Aircraft Establishment for his study of 15th-order resonance.

After discussions with NASA/Goddard Space Flight Center (GSFC) and the Naval Research Laboratory (NRL), the NTS-1 satellite was dropped from the Baker-Nunn tasking roster as of 31 May. No laser ranging to this object was attempted by the SAO network because of a persistent satellite-tumbling problem.

The Baker-Nunn camera in Australia remains in storage, awaiting transfer to a new facility in Orroral Valley. This camera will be operated in conjunction with the laser system, which will be moved from Olifantsfontein, South Africa, to Australia. The Baker-Nunn camera now in South Africa will be operated by the Canadian Forces (CF) in St. Margaret's, New Brunswick, Canada, under a cooperative agreement with SAO. The twelfth camera remains on loan to the CNES in Ouagadougou, Upper Volta, where it commenced part-time operations in support of D5B in June.

Table 2. Total number of Baker-Nunn observations.

Month	Number of observations
January	955
February	787
March	771
April	952
May	1680
June	1083
Total	6228

Table 3. Successful observations on atmospheric satellites.

Satellite	Jan.	Feb.	March	April	May	June	Total
Vanguard 2	50	38	58	62	158	74	440
Explorer 8	62	57	38	14	38	28	237
Explorer 19	182	23	91	85	166	119	666
Explorer 32	21	47	1	59	41	15	184
Explorer 39	3	27	108	7	58	97	300
Total	318	192	296	227	461	333	1827

2.4 Laser Upgrading

2.4.1 Pulse-processing system

In early January, the prototype version of the pulse-processing system at Mt. Hopkins was modified to the production version of the new system. It has been operational since that time. The production systems for Brazil and Peru have been assembled and checked out at Cambridge and have been shipped to their respective destinations. The Brazil system is on site at Natal, while the one for Peru is in transit. A special requirement by NASA for intensive tracking of Geos 3 for the next few months has affected the original schedule of upgrading the pulse-processing system at each station. As a result, stations will be upgraded when seasonal periods of poor tracking weather occur. Brazil will be upgraded in July, and Peru at the beginning of CY 1976. Installation of the fourth system will be delayed until the laser is installed at Orroral Valley, Australia, in the early part of 1976.

In general, no major problems have occurred with the pulse-processing system; however, a problem was discovered in the Nanofast counter. The specified short-term accuracy of 0.1 nsec claimed by the manufacturer for the counter was not realized when the counter was operated from the external 1-MHz clock provided by the station frequency standard. The problem was traced to phase jitter in the frequency multiplier in the Nanofast counter, which reduced the short-term stability to about 0.4 nsec. The counter does provide a short-term accuracy of 0.1 nsec if an external 10-MHz clock frequency is used and if the problem multiplier is bypassed.

To operate in this mode, we have purchased multichannel distribution amplifiers for the four laser systems. These also contain 1-MHz amplifiers, which will be used to improve the distribution of the 1-MHz signals required by other portions of the system.

After analyzing the large quantity of calibration data obtained from Mt. Hopkins, sufficient confidence has been gained regarding the stability of the

laser ranging system. This has resulted in a great reduction in the numbers of calibration data required. Study of the short-term stability of the pre-target and post-target ranging calibrations continues.

Programs to process calibration data on the minicomputers at the stations have been written and implemented at Mt. Hopkins.

The equipment modification that allows the laser to pulse at 8 pulses per minute (ppm) has been incorporated and is operational at all laser stations. This step was an important one in the overall program of upgrading the SAO laser systems. Table 4 lists the dates the modification became operational at each site.

2.4.2 Field minicomputers

During the first 6 months of 1975, one of the major phases of the laser-upgrading program was completed. All four field minicomputer systems were installed at the laser sites (see Table 4), and personnel have been trained in their use. The systems are now routinely generating predictions locally by means of prediction software developed and tested during the period. The development of field processing software for the minicomputer systems continues. In June, programs to copy paper tapes to Linc tape and to select subsets of quick-look data for transmission to Cambridge for orbital maintenance were completed. These routines will reduce teletype traffic from the field by up to an order of magnitude.

2.5 Engineering

2.5.1 Timing

All SAO laser stations have maintained their clocks recoverable to ± 10 μsec relative to UTC (United States Naval Observatory, USNO). The laser/Baker-Nunn stations in Greece and Japan have maintained time recoverable to ± 25 μsec relative to UTC (USNO), and the Baker-Nunn stations in Spain and Hawaii, to ± 50 μsec. India and Ethiopia are set to WWV-HF timing signals, and their timing uncertainty is estimated to be ± 1 msec.

Table 4. Operational dates, laser-upgrading program.

Station	Minicomputer-generated predictions	8-ppm modification
Arizona	7 January	18 January
Brazil	4 February	4 February
Peru	25 March	16 April
South Africa	30 April	30 April

After clock comparisons were made at Greece, Hawaii, Mt. Hopkins, Peru, South Africa, and Spain, the master clocks at these stations were reset. Comparisons at Brazil, India, and Japan are planned for the near future.

Brazil has installed a complete backup clock system with its own rubidium frequency standard. Peru has been shipped a second rubidium frequency standard for its backup clock system.

The Loran C equipment in Greece has been calibrated, and transmitting stations 7990-M, 7990-X, and 7990-Y are monitored. The Japan Loran-C equipment monitors 9970-M. Since the West Coast Loran D experimental system has been moved to Norway, Mt. Hopkins is no longer able to monitor a reliable Loran signal. This station compensates for this change by means of monthly clock comparisons.

We have decided to purchase and deploy Timation time-transfer equipment in Brazil and Peru and expect to field the equipment in late CY 1976.

2.5.2 Pulse chopper

In February, SAO awarded a contract to Lasermetrics, Inc., of Teaneck, New Jersey, to design and manufacture an optical pulse chopper. The chopper is a fast optical shutter placed between the laser oscillator and the amplifier to decrease the laser pulse width from the present 20 nsec to a nominal 5 nsec. A shorter laser pulse will result in increased ranging accuracy. Field acceptance testing is scheduled for July in Arizona. We are planning to purchase three more choppers for our other laser systems after the first unit has been successfully tested.

2.5.3 Arizona mount refurbishment

In January, SAO started a major refurbishment of the Arizona laser mount to increase its pointing accuracy and reliability. The automatic drive-train housings were redesigned and are being rebuilt. Worn and damaged parts, such

as the main worm gears, will be replaced. The refurbishment is scheduled to be completed by the end of November.

2.6 Laser System Accuracy

Under the current laser-upgrading activities (see Sections 2.4 and 2.5), the ranging accuracy of the SAO lasers is being improved to meet program requirements. The present upgrading program is intended to yield 10-cm ranging accuracy for low-orbiting satellites during the tenure of the Geos 3 project.

Before this work was initiated, the ranging accuracy was about 50 cm to 1 m, based on ground target measurements. The major error sources at that time were 1) return-pulse waveform distortion, 2) laser pulse width, 3) laser wavefront distortion, and 4) station timing. These effects have previously been discussed in detail (Pearlman et al., 1975; see also Proposal to NASA for the Upgrading of SAO Laser Systems, P 423-5-73 Supplement No. 1, NASA Grant NGR 09-015-002, January 1974). Although upgrading activities are at an interim stage, some system improvements have already shown a very positive effect on range accuracy.

The implementation of the pulse processor (Section 2.4.1) has reduced range noise by a factor of 2 to 3. Figure 1 shows an example of such improvement on a typical pass of data. Even more important, however, the pulse processor has also reduced the large systematic range errors that result from variations in signal amplitude due to changes in satellite range and cross section. Comparisons were made between the original laser fixed-threshold pulse-detection system and the new pulse processor. Using short-arc analyses on both sets of data, we examined computed orbital differences. Some typical examples of the results are shown in Figures 2a, b, and c. Excursions as large as several meters are apparent in many of the cases, and changes of sign are also very common. These results are similar to comparisons made on ground targets. It should be realized,

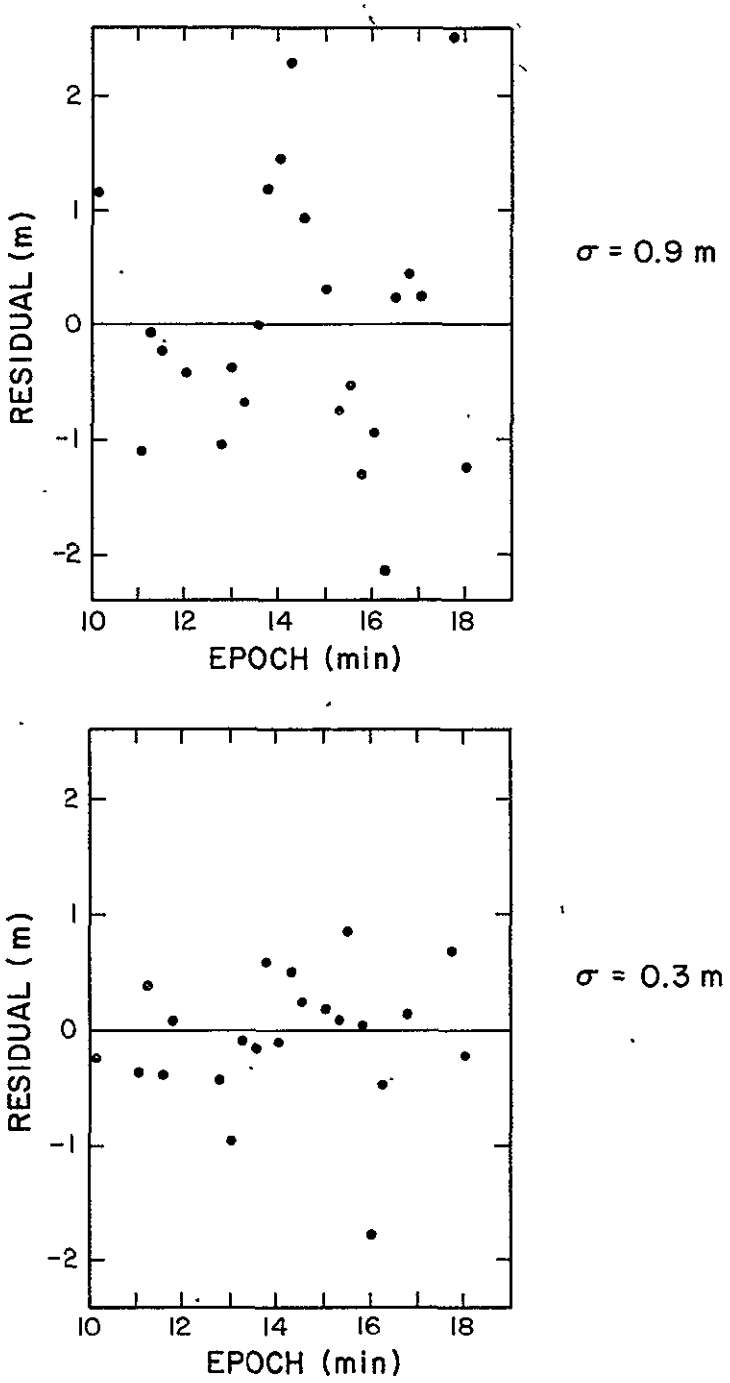

Range residuals to a short arc orbital fit on Beacon-C (30 Nov. 1974, 11^h10^m UT).

Figure 1. Range residuals to a short-arc orbital fit on BE-C (30 November 1974, 11^h10^m UT). Upper diagram is with the use of the original threshold; lower diagram, with the new pulse processor.

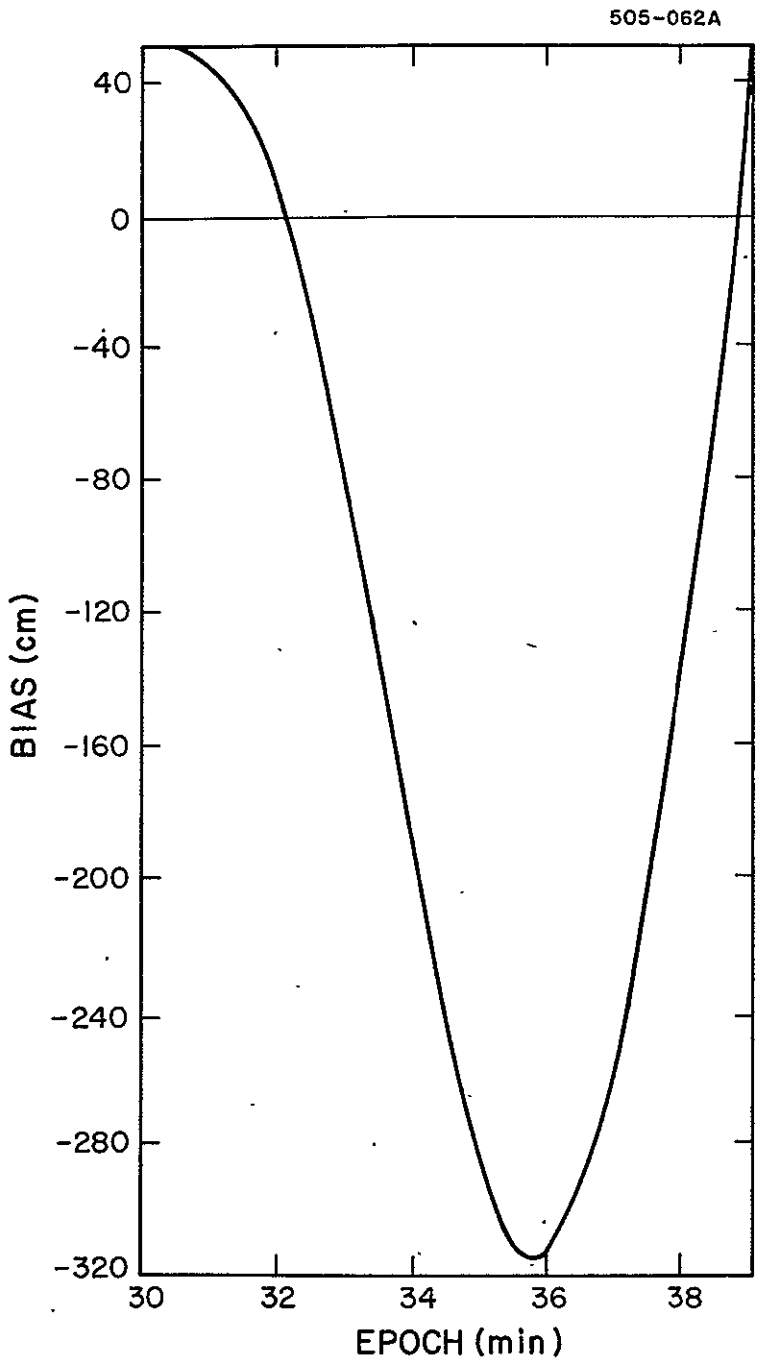

Figure 2a. Range bias (old system minus new system) from the transit of Geos 1 on 30 November 1974 at 3^h30^m.

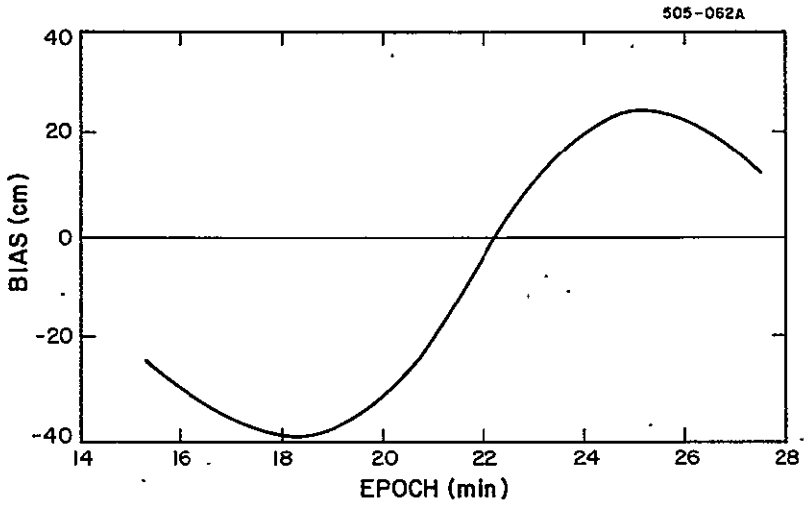

Figure 2b. Range bias (old system minus new system) from the transit of BE-C on 11 December 1974 at 9^h15^m.

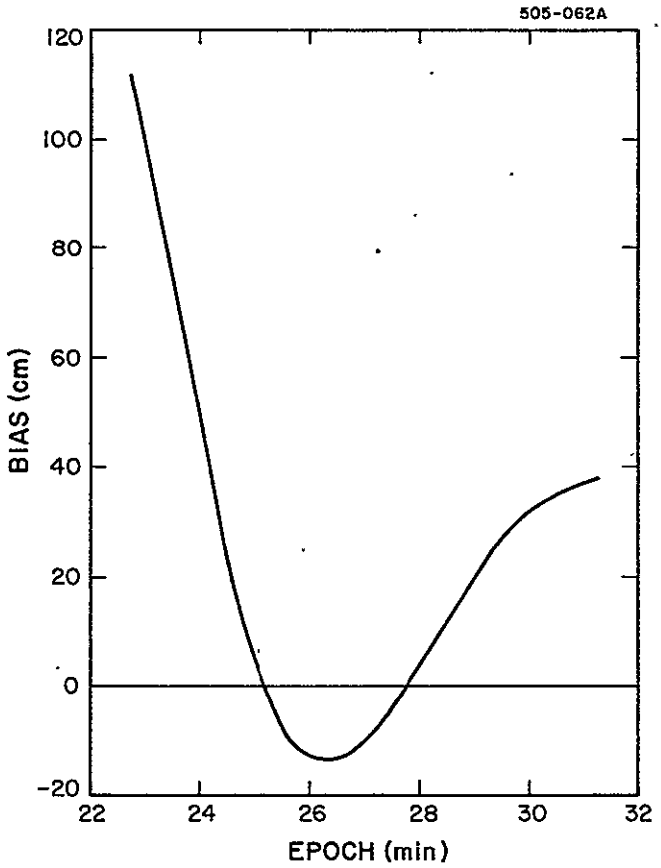

Figure 2c. Range bias (old system minus new system) from the transit of BE-C on 8 December 1974 at 11^h22^m.

however, that short-arc analyses may introduce some of the signature characteristics, and the total excursions may not be due to the detection systems alone.

Target measurements and electronic calibrations indicate that the pulse processor and its operation are compatible with ranging accuracies of considerably better than 10 cm. Target calibrations taken before and after individual satellite passes have been used to estimate system stability. The difference in these precalibration and postcalibration values is typically 1 nsec or less (see Figure 3). However, most of this difference can be accounted for by the 25-nsec laser pulse width itself. Since these are measurements on a flat target, the influence of wavefront variations has been averaged out.

Electronic measurements show that the pulse-processing system itself is stable over the long term to a few tenths of a nanosecond.

With the deployment of the pulse processor, the dominant sources of error lie now with pulse width and wavefront distortion, which have a combined influence of about 20 to 30 cm. An optical pulse chopper (see Section 2.5.2) is being tested as a means to reduce these effects. Although the system has not yet been implemented, it should provide us with the factor-of-three improvement necessary to reach 10-cm ranging accuracy.

Improvements in station timing have come about through the use of rubidium oscillators and better time-reduction procedures. Timing accuracy is now about 10 to 20 μsec (traceable to USNO) (see Section 2.5.1). Under the current plan, Loran receivers, which will be available from GSFC in early 1976, will be used to ensure better than 10 μsec at the stations. Two Timation receivers are scheduled for delivery in late 1976; these are slated for our most remote stations, Brazil and Peru, and will provide 1-μsec timing accuracy.

2.7 Communications

Radio communications from January to May were seriously degraded by a newly constructed power-distribution center immediately adjacent to the SAO

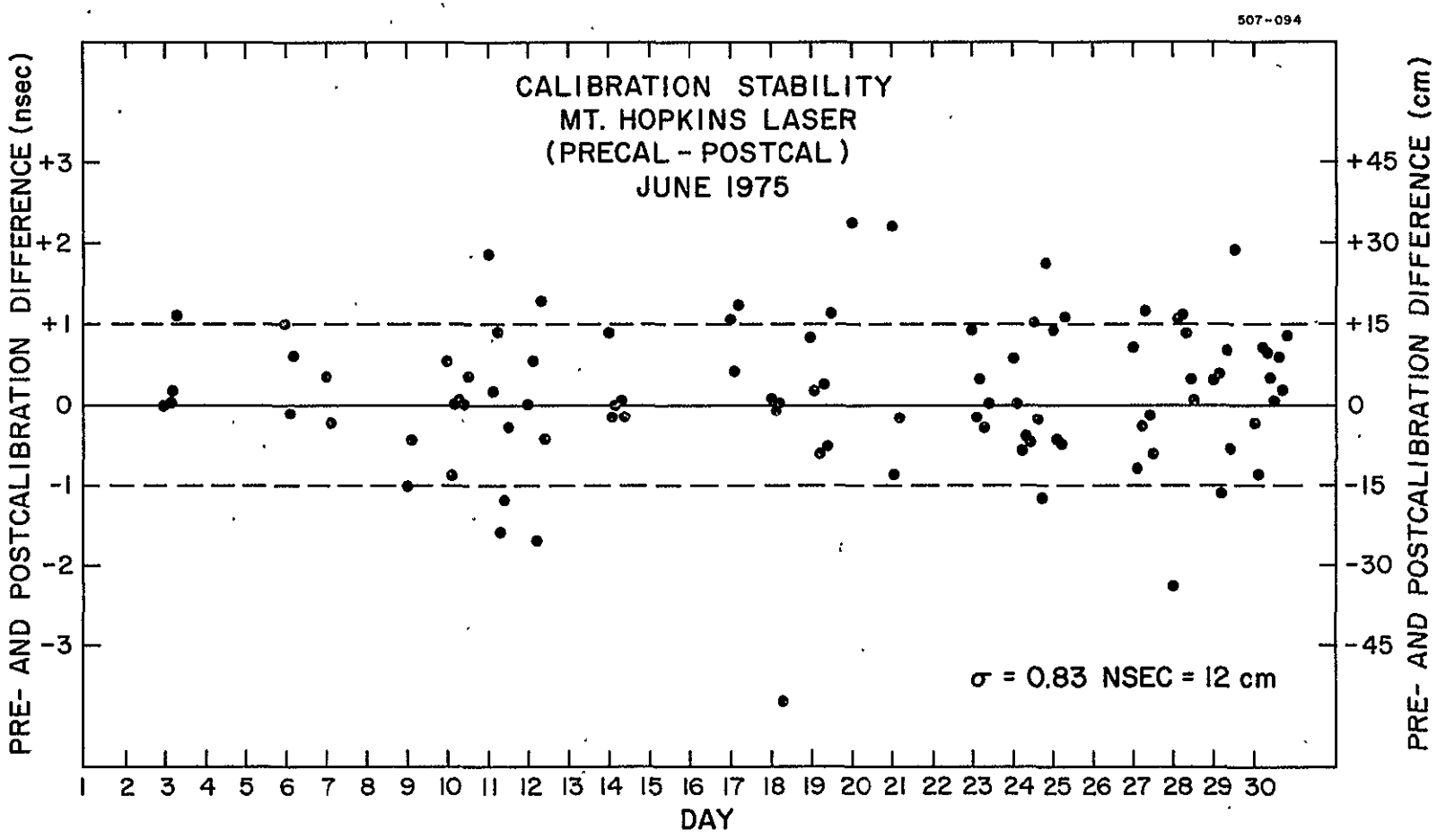

Figure 3. Calibration stability of the Mt. Hopkins laser: precalibration minus postcalibration.

Communications Center. The source of interference was isolated and is now being corrected by the Boston Edison Company.

Two ASR-28's and a receive-only teletype machine, acquired from GSFC and now in use, have increased the efficiency of the SAO Communications Center.

2.8 Data Services and Programing

2.8.1 Software

Responsibility for processing incoming data from the new pulse-processing systems was turned over to the Data Services Division in February, and work continued on developing the CDC 6400 production processing system for the new data. This program will incorporate software already developed. The satellite portion of the program was modified to accommodate a new model that will more accurately reflect systems delays. The target-calibration portion was enlarged, and the latest system-calibration models were incorporated. In June, revisions to the program were completed and put into production. Additionally, the program is capable of batch processing a large number of satellite passes. The output format was changed to provide greater ease in scanning the data, and further modifications to the target-calibration model were initiated and completed during the same month.

2.8.2 Data-handling system

In March, the data-preprocessing program was modified to enable it to accept new formats from the pulse processor. Subsequent modifications enabled it to diagnose and display systems and operational errors on the pulse-processor during routine operation.

2.8.3 Minicomputer for Data Services

A minicomputer system for the Data Services Division was ordered in February and delivered the following month. This system will be used to process field data and will serve as a backup for systems in the field.

2.8.4 Routine operations

Table 5 lists the satellites for which orbital elements and predictions were computed by the Data Services Division during this reporting period. For use in generating laser predictions, orbital elements were provided on BE-C, Geos 1, Geos 2, Starlette, and Geos 3 for the laser sites at Mt. Hopkins, Brazil, Peru, TAO, Air Force Cambridge Research Laboratories, Institut für Angewandte Geodäsie in Germany, and CNES. Pointing predictions for these same satellites were supplied to NTU. Camera predictions were generated and sent to 10 Baker-Nunn sites.

Orbits and predictions were provided to the Baker-Nunn sites on three satellites as cooperative effort: 1971 54A in support of King-Hele's research, 1975 33A (Aryabhata) for India, and 1975 39B for CNES.

Laser data through December 1974 were validated and made available for analysis. Computer programs have been revised to handle the large volume of data now being received.

Reference System Bulletin No. 3, including data through December 1974, was completed and is in press.

Skylab predictions continue to be generated for public information.

The film-control section received and cataloged 7179 observations on 4382 films from the SAO Baker-Nunn stations; 411 films were obtained from the Air Force sites.

Table 5. Satellites tracked from 1 January through 30 June 1975.

Satellite		Name
	Tracked on Request from NASA	
1963	53A	Explorer 19
1965	89A	Geos 1*
1968	2A	Geos 2*
1975	27A	Geos 3*
	Tracked for Geodesy and Earth Physics	
1964	64A	BE-B
1965	32A	BE-C*
1965	89A	Geos 1
1968	2A	Geos 2
1970	109A	Peole
1975	10A	Starlette*
	Tracked for Long-Period Perturbations	
1959	$\alpha 1$	Vanguard 2
1960	$\iota 2$	Echo 1 Rocket Body
1964	64A	BE-B
1965	89A	Geos 1
	Tracked for Atmospheric Investigations	
1959	$\alpha 1$	Vanguard 2
1960	$\xi 1$	Explorer 8
1963	53A	Explorer 19
1966	44A	Explorer 32
1968	66A	Explorer 39
	Special Requests	
1971	54A	Thor Burner 2 Rocket
1974	54A	NTS-1
1975	33A	Aryabhata
1975	39B	D5B

*Satellites ranged by lasers during this 6-month period.

A total of 1883 satellite positions were precisely reduced, bringing the number of all reductions to 246,860 as of 30 June 1975. Table 6 gives a breakdown of the precise reductions during this period.

2.8.5 Closing of the photoreduction facility

The SAO photoreduction facility was closed on 30 June, there no longer being a strong requirement for photoreduced Baker-Nunn data. Photoreduction in support of upper atmospheric research will continue at the University of Bologna, Italy, under a cooperative program with SAO.

2.8.6 Disposition of Baker-Nunn film

A plan has been formulated to dispose of unneeded Baker-Nunn films and to store the remainder under a regular disposal schedule at the Federal Records Center in Waltham, Massachusetts. In addition, contemporary film will be disposed of at the stations, except for those on a few selected objects or special observations. This plan will be implemented in the fall of CY 1975, pending discussion with and agreement of the SAO scientific staff and the international scientific community.

2.9 Special Experiments

Special experiments are being conducted in the area of analyzing the operating performance of the SAO laser systems. Range calibration is being investigated to develop system models for use in data processing and analysis. The study of possible sources of an observed discrepancy between measured and calculated signal strength continues. In April, radiometer tests were performed at Mt. Hopkins in an effort to isolate the source of this discrepancy; however, results were inconclusive during this report period owing to an apparent inconsistency in the data obtained. These experiments are supported

Table 6. Reductions completed 1 January through 30 June 1975.

Object	Period	Number of images	Investigator
Explorer 19	May through December 1973	1204	Dr. Jacchia
Geos 1 Geos 2	June 1972 through July 1973	679	Dr. E. M. Gaposchkin
	Total	1883	

jointly by the Office of Tracking and Data Acquisition and the Office of Applications, and details are reported in Section 3.8 below.

2.10 Personnel

During this period, Mr. William Johnson, an observer, transferred from the station in Natal to a temporary assignment at Olifantsfontein. Johnson expects to remain there, increasing station manpower in support of the Geos 3 campaign, until the station ceases operation this calendar year.

In April, Mr. Donald S. Patterson joined SAO as an assistant observer on the Mt. Hopkins station staff. A Tucson resident, Patterson majored in electrical engineering at local Arizona colleges.

The following month, Mr. Ilo G. Cambell joined the Department's programing staff to work on software development for the minicomputer system. Campbell has been employed at SAO since 1958, serving as an observer in Spain and most recently as a mathematician and programer with the Upper Atmospheric Research Group.

Mrs. Shwen-I. Yeh, a native of China, joined the staff of the Experimental Geophysics Department in May, where she is a data assistant with the Data Services and STADAD groups.

Mr. Hildegondes Fernandes, a Brazilian National employee, left the Natal station staff. A replacement was sought through the Instituto Nacional des Pesquisas Espaciais, our local cooperating agency.

Mr. Albert Werner, Chief of the Moonwatch Division, retired on 30 June 1975 at the close of the Moonwatch program. Werner joined SAO in 1965 and served as Chief of Moonwatch for 7 years, the longest tenure of anyone in that position.

Several of the field and headquarters staff participated in training courses during the report period. These sessions included hands-on technical and theoretical training, seminars in engineering design, and courses in minicomputer hardware and software. The minicomputer training was provided under the equipment purchase contract with Data General Corporation. In addition, some of the Headquarters staff attended an Equal Employment Opportunity seminar presented in Cambridge by Smithsonian Institution (SI) in May.

2.11 Special Projects

2.11.1 South Africa station move

We obtained approval from NASA to relocate the laser system now operating at Olifantsfontein, South Africa, to Orroral Valley, Australia. Our cooperating agency there, the Australian Department of Science (DOS), plans to construct facilities to house the laser and Baker-Nunn camera (formerly located at Island Lagoon, Australia) in proximity to the NASA minitrack facility on the valley floor. These facilities will be built with funds jointly provided by NASA and DOS. The new station will be under the direction of Mr. Dennis Willshire, Orroral Valley Station Director, and will be staffed by Australian personnel and one senior United States technical representative.

A loan agreement between SAO and CF for the operation of the Baker-Nunn camera now at Olifantsfontein was drafted and sent to CF for signature. CF plans to operate the camera at its site in St. Margarets, New Brunswick.

The South Africa site, where the equipment is now located, will be closed and vacated by 31 December 1975. The camera and the laser should be operational at their new locations in early calendar year 1976.

2.11.2 Hawaii station property

A fire early in the morning of 1 February destroyed the dormitory and kitchen facilities of the Mt. Haleakala Hawaii Astrophysical Observing Station

and caused the roof of an adjoining building to cave in. No personnel were injured. The fire was contained in those areas, and no damage was done to station equipment or equipment housing. The cause of the fire was unknown, but it was probably the result of faulty electrical wiring. The site has been cleared, and all rubble removed. There are no plans to reconstruct the lost facilities.

2.11.3 Moonwatch

The SAO Moonwatch Program, pioneer space network of volunteer observers, ceased operations on 30 June 1975, after more than decade and a half of success. A special commemorative ceremony honoring the program's many accomplishments was held in the Presidential Reception Room of SI's National Museum of History and Technology on 26 June. Attendees included dignitaries from NASA and SI and persons historically associated with the program, including its founder and former SAO Director, Dr. Fred L. Whipple. A prototype Moonwatch telescope was presented to Mr. Fred Durant, Assistant Director, Department of Astronautics, for the permanent collection of the new National Air and Space Museum.

3. SATELLITE GEODESY AND GEOPHYSICS PROGRAMS

3.1 Introduction

During the period 1 January to 30 June 1975, research has been directed toward studies of the dynamics of the solid earth as related to Earthquake-Hazard Assessment (EHA) models in support of NASA's Earth and Ocean Dynamics Applications Program (EODAP). According to objectives delineated in SAO's Research and Technology Operating Plans (RTOP), divisional efforts have included improvement of satellite ephemerides; use of existing satellite-tracking data for the determination of geophysical parameters, such as the gravity field, earth tides, polar motion, and station location; reduction and analysis of geodimeter measurements to determine local movements of the earth's crust; and studies to establish requirements for satellite-tracking equipment, network distribution, and satellite design.

The scientific work related to individual RTOPs is discussed in the following subsections.

3.2 Geophysical Data Base (RTOP 369-01-04)

The computerized Geophysical Data Base (GDB) has been designed and constructed. Containing all available data appropriate for the earth-dynamics applications area of EODAP, the GDB fulfills a need at SAO for a system to manage the vast amount of data used in our analyses.

Among the factors we considered in establishing such a base were the quantity of data available and the resolution required for cataloging.

Many data relating to the earth's lithosphere are already available in computer-accessible form, and increasing amounts are expected to result from future research. Some typical current data include surface gravity, heat

flow, topographic height, crustal thickness, seismic-velocity profiles, density variations, earthquake history, and plate motion. These data are mostly numerical, but future data may be of a descriptive type and may include word descriptions. In general, the data are complex enough to require tabular compilations.

To estimate the numbers of data involved, we first had to determine the desired geographical resolution. The finest resolution to be cataloged had to be small enough to distinguish geological detail but large enough to give a manageable number of data points. For current scientific applications, areas of 100 km X 100 km, roughly 1° X 1°, seemed to satisfy these conflicting criteria best. This means approximately 4×10^4 data points. Assuming an average of 80 characters per data point for each of 30 to 3000 types of data, the estimated amount of data involved is 10^8 to 10^{10} characters.

In addition, the GDB was designed to fulfill other requirements. Owing to the large numbers of data and potential users, automatic file management was indicated — to maintain records of where and how the data are stored, to provide for protection and backup of data files, to facilitate changes or additions to the data, and to keep users informed of such changes. Because the full scope of future use could not be predicted, it was important that there be few limitations on the structure and format of the data. The possibility of remote users suggested that the system should be made available through an interactive as well as a batch system. Finally, as is true for any system that will be in use for many years, it was desirable that the system be machine transferrable.

Thus, the first major task was to develop a data file structure and a system for managing the data. The results of this completed effort have been published in a report (Williamson and Kirschner, 1975) that also serves as a users' guide and as a subroutine documentation.

Designed to have maximum flexibility compatible with our immediate requirements, the GDB has evolved into a general data-management system appropriate to a wide range of needs. The GDB provides efficient random access of

many (up to disk capacity), large (up to 1.5 X 10^6 characters) subsets of a large (up to the number of magnetic tapes available) conglomerate of data. The system also offers file-management capabilities, including protection of the data. The GDB does not assume particular formats for data records. It could easily be a basic tool for designing a group of data sets with a more complex and specialized organization.

Since the data will be used in many ways for several related projects, a random-access capability was needed. A critical requirement, then, was for random access of 10^8 to 10^{10} characters, thus dictating a dual system that uses magnetic tapes for permanent storage and disk files for temporary storage.

The GDB operates on the CDC 6400 computer. An interactive capability can be provided by the Intercom system. The GDB should be easily transferable to other modern computing systems with tape and disk facilities and a Fortran compiler. The GDB subroutines are written in Fortran except for some basic input/output routines coded in Compass, which would need to be reprogramed for use on another computer.

Software for the GDB now includes a subroutine that recovers data files residing on tape after the respective catalog entries have been overwritten.

3.3 Tectonic Plate Motion and Fault Motion (RTOP 639-02-01)

To provide data for an EHA model, an experiment was undertaken during the reporting period to investigate the possibility of direct measurements of the relative motion of tectonic plates across intercontinental distances. Figure 4 is a tectonic map of the world showing major plate boundaries and their relative rates of motion. We see from the figure that 1) relative plate motions are significantly faster in the equatorial regions than in the polar regions, 2) the fastest relative motions tend to be in the east–west direction, 3) the fastest motions are between plates composed entirely of oceanic lithosphere, and 4) the largest relative plate motion on the earth occurs between the Pacific and the Nazca plates at rates up to 18 cm $year^{-1}$.

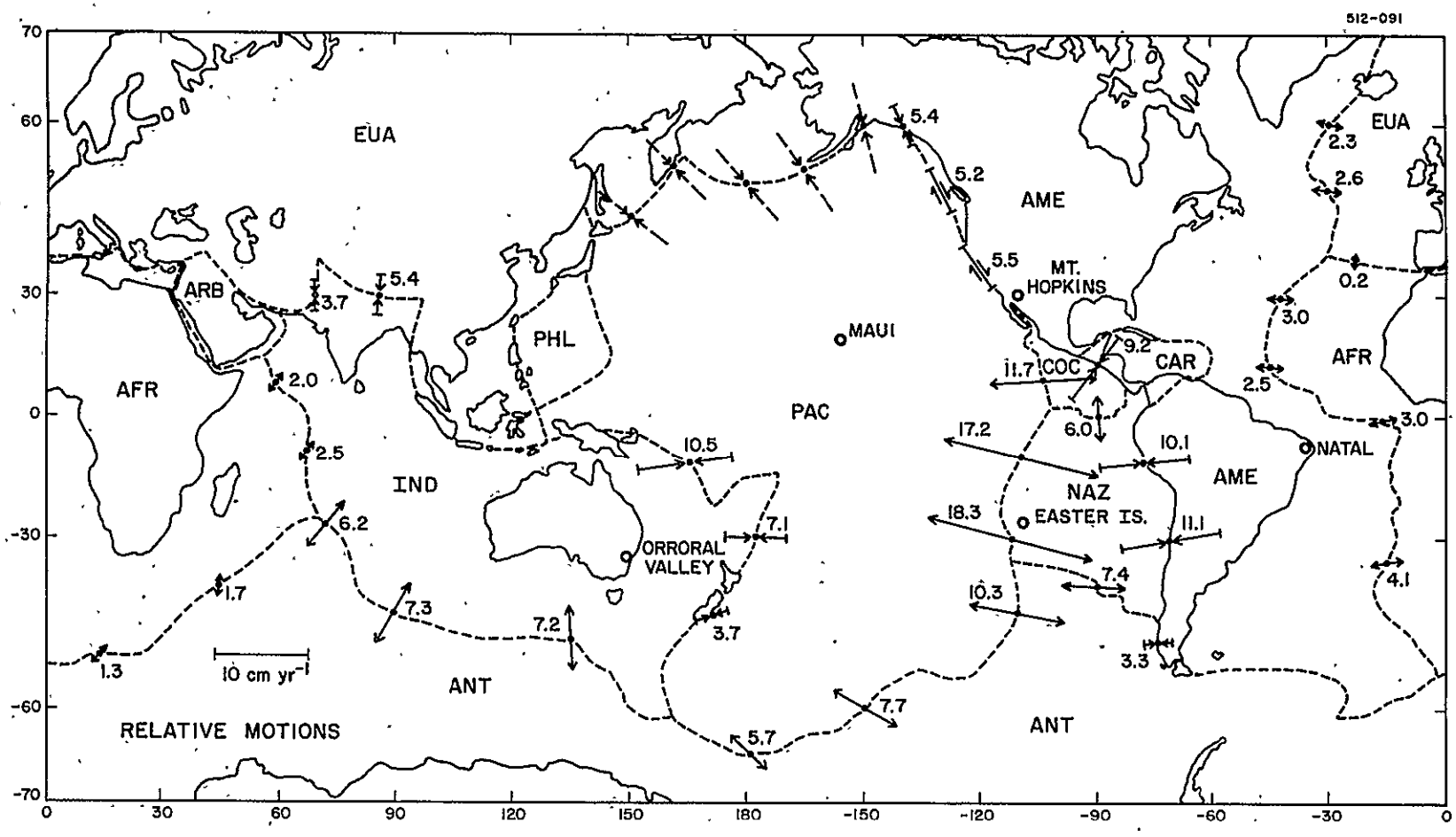

Figure 4. Outline of the plates (dashed lines). AFR: African, AME: American, ANT: Antartic, ARB: Arabian, CAR: Caribbean, COC: Cocos, EUA: Eurasian, IND: Indian, NAZ: Nazca, PAC: Pacific, and PHL: Philippine. The relative motions of the plates are shown by arrows, in cm year^{-1} (after Minster, Jordan, Molnar, and Haines, 1974, model RM1).

With the purpose of measuring baselines across the world's fastest accreting and subducting plate boundaries, and bearing in mind economic and logistics constraints, Drs. Gaposchkin, N. H. Mao, and Paul A. Mohr suggested a network with Easter Island, on the Nazca plate, as the focal point. Other stations proposed for this network include the existing SAO stations of Orroral Valley, Australia, located on the Indian plate; Mt. Hopkins, Arizona, on the North American plate; Maui, Hawaii (laser equipment would have to be added to this existing Baker-Nunn camera station), on the Pacific plate; and Natal, Brazil, on the South American plate. Typical rates of motion in each of these directions from the East Pacific Rise have been estimated to be between 10 and 15 cm $year^{-1}$. The crucial station site in our plan, Easter Island lies far enough from the epicenters of the East Pacific Rise to be utilized. Additional precise terrestrial geodetic monitoring of the island would detect any local deformations.

Mao and Mohr undertook a geological and geophysical evaluation of the proposed sites in terms of their tectonic stability. A literature search revealed no major problems associated with locating a laser tracking station and necessary instrumentation at the potential sites. They are investigating the geophysical aspects of the plate-motion experiment and the justification of having supplementary geodetic and geophysical measurements.

Precise laser ranging to satellites is well-suited for measuring instantaneous plate motions at all types of plate boundaries. Supported by a careful observation program and with the use of gravimetric and microseismic surveys, tiltmeters, and gravimeters to detect local crustal deformation around the laser stations, the results of the project can be validated and interpreted. Specifically, a geodetic survey would resolve local horizontal ground deformations above a threshold of approximately 5 mm, while a microseismic survey would continuously monitor the microseismicity in the vicinities of the stations, allowing us to determine whether consistent uniformity exists over a large area of a plate.

With a gravimeter, we can measure diurnal earth tides with peak-to-peak amplitudes of to 20 to 30 cm. In addition, by means of a tiltmeter, we can detect local tilts owing to meteorological, insolation, tectonic, and other causes. Sensitive gravimeters can monitor vertical changes in elevation to approximately 4 cm.

Drs. Paul Kalaghan and Gaposchkin and Ms. Margaret Anderson have been conducting a simulation to study the amount and accuracy of precise laser observational data required. The approach taken has been as follows. First, a nominal satellite orbit is specified and employed to generate a set of simulated laser observations from each station in the network under consideration. Second, an error model is defined to represent the uncertainties present in the actual observations. With these observations and the error model as input data, the precision orbit-computation program is employed to determine, in an iterative manner, both the orbit of the satellite observed and the positions of the stations conducting the observations. The process is begun by inputting nominal values of all variables under study. Analysis of the successive estimates of the numerical value of each of these variables from one iteration to the next then forms the basis of a method to determine the effects of model uncertainties (e.g., noise in the data or uncertainties in the gravity-field coefficients) on the accurate locations of the stations comprising the observing network.

Consider now the specific details of the simulations carried out. Lageos and Starlette were employed as the satellites to be observed (see Table 7). With Easter Island as the focal point, the simulation included the 10-station network shown in Figure 5. The error model utilized to generate the various noise components corrupting actual observational data included the following:

A. A gravity-field error model of

$$\delta\bar{C}^{*}_{\ell m} = A \times 10^{-9}\, \ell^{0.3} \quad , \quad \ell \leq 6 \quad .$$

Table 7. Orbital elements used in the simulation.

Orbital element	Lageos	Starlette
a	12.240 mm	7.335 mm
e	0.01	0.02
I	110°	50°
ω	-0°.2109 day^{-1}	3°.3 day^{-1}
Ω	0°.3473 day^{-1}	-3°.9 day^{-1}
n	6.40 rev day^{-1}	13.82 rev day^{-1}

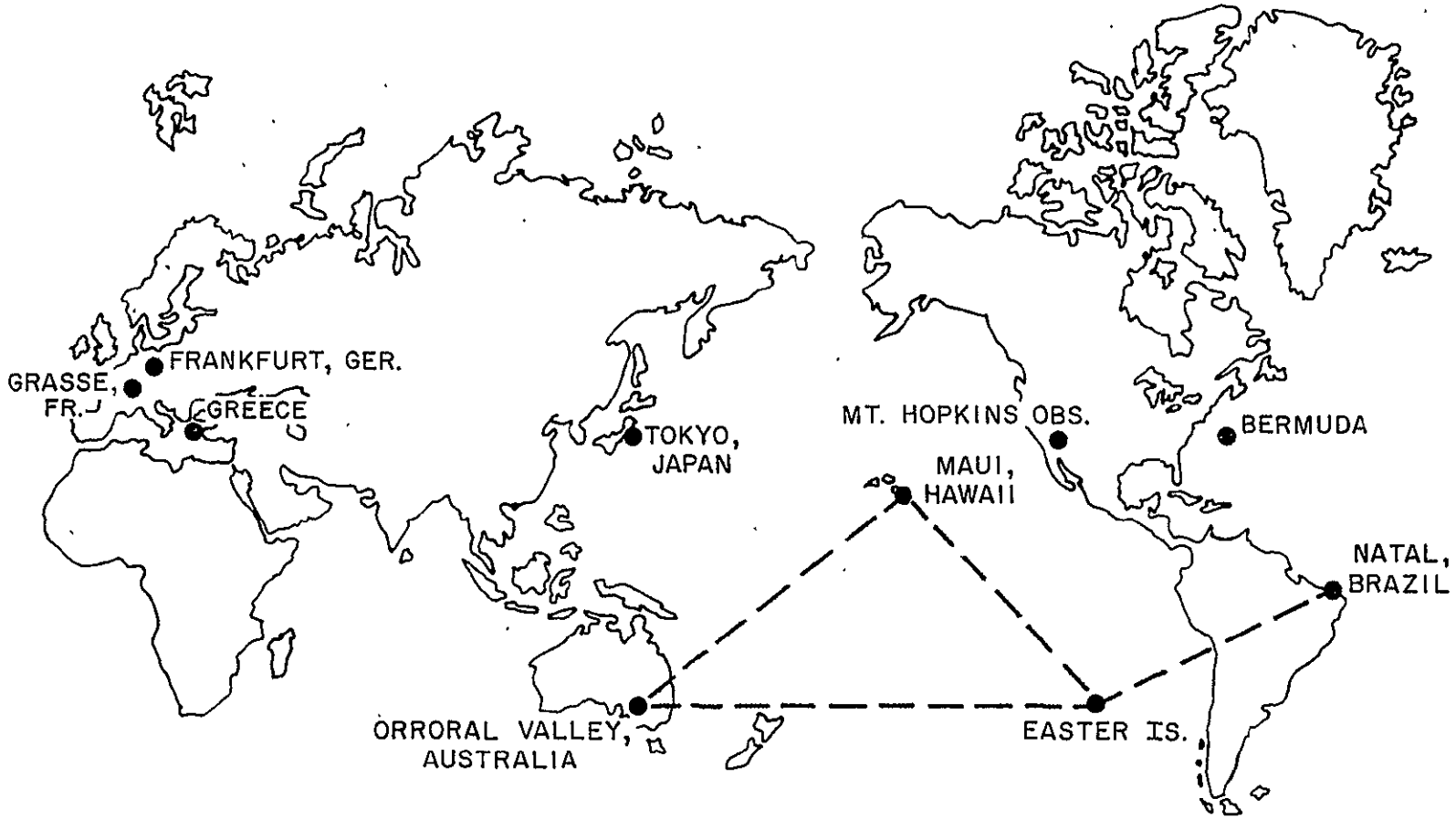

Figure 5. Station configuration for simulation of detection of plate motion.

B. A station-coordinate error of ±1.5 m.

C. A laser-data error of ±5-cm bias, random from pass to pass, and ±5-cm noise, random from point to point.

Observations for the Lageos orbit were generated over a 5.5-day period at intervals of 2 min, a period chosen to allow at least 16 passes over Easter Island. The numbers of passes for the other stations ranged from 7 for Natal to 20 for Frankfurt and Grasse. For Starlette, the observation period was extended to 10 days. This increased the number of Easter Island passes to 33, while for the other stations the minimum number of passes was 27 (Natal) and the maximum was 47 (Grasse). The simulated observations incorporating the above error models were then processed by the precision orbit-computation program to yield simultaneous solutions for the coordinates of all stations. The resulting root-mean-square (rms) deviations in all the coordinates in the solution are displayed in Table 8 as function of A, the magnitude of the gravity-field error model. The data in this table are plotted in Figure 6. The most pronounced feature of these results is the dependence on satellite height. As the satellite orbit decreases in altitude, the effect of the gravity-field errors is significantly amplified. In order to obtain a nominal 5-cm $year^{-1}$ accuracy, a ±5-cm error in each set of 5-day observations would indicate a maximum allowable gravity-field error amplitude of A = 1.0 for Lageos and A = 0.1 for Starlette. Also shown in Figure 6 are the error bars representing the standard deviations of each of the rms station-displacement values shown. These values were based on a five-case sample in which equivalent but statistically independent parameter uncertainties were employed to determine five separate rms station-displacement values for each of the tesseral error distributions implied in the legend to Figure 6. As a measure of the magnitude of ϵ, it should be noted that the errors in SE III can be represented in Figure 6 with an ϵ value between 5 and 10.

Also during this reporting period, Gaposchkin and Mr. James Latimer began a series of simulations of the laser multilateration technique to determine whether this method can be used to validate the Lageos tracking system and to

Table 8. rms station-coordinate errors (m), based on the error model given in Figure 6.

Satellite	A = 0	A = 2.5	A = 10
Lageos	0.06	0.15	0.40
Starlette	0.08	1.70	6.95

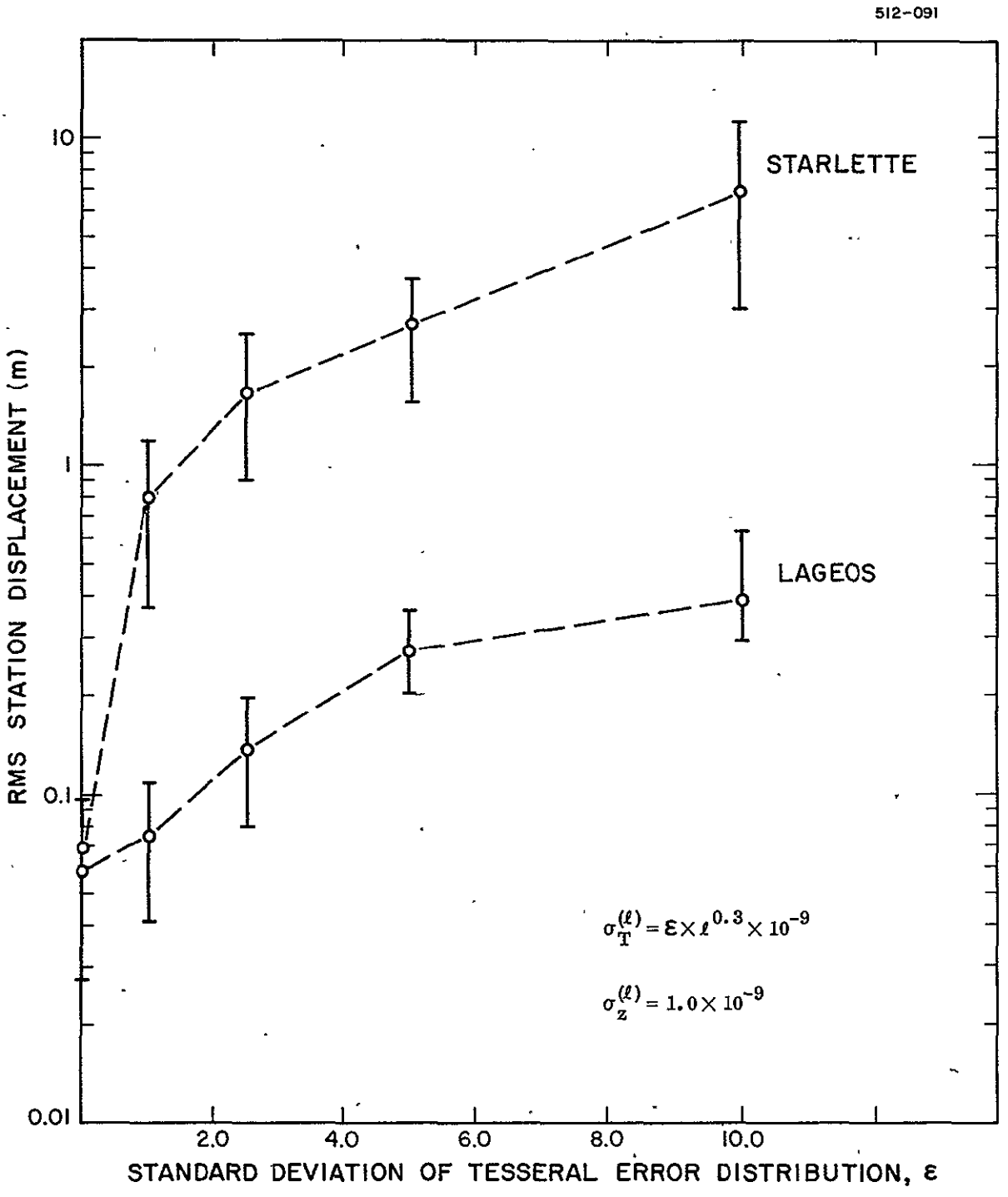

Figure 6. rms station-position errors versus the gravity-field error amplitude.

investigate whether multilateration is a viable supplement to orbital techniques — specifically, whether station coordinates with an accuracy of 5 cm can be obtained. Based on results of a simulation, simultaneous observations of both Lageos and Starlette can be made by use of the following stations: GSFC, Greenbelt, Maryland; Grand Turk; Bermuda; Patrick Air Force Base, Florida; McDonald Observatory, Texas; and Meades Ranch, Kansas. Ten tracks of satellite data were generated — six of Lageos and four of Starlette. Each track consisted of 21 satellite positions separated by 2° of true anomaly for Lageos and 1° for Starlette. The tracks represent possible trajectories of the satellites; they were not generated at random but rather located deliberately in a reasonably well-distributed way over the region of mutual station visibility. Errors were then introduced to represent a 5-cm pass bias (random from pass to pass but constant within a pass) and 5-cm noise. Solutions were computed for six stations, and then for five and four. Two-satellite solutions and a Lageos-only solution were made. The measure of goodness was chosen to be the rms of the interstation baseline errors resulting from the solutions. The results are displayed in Table 9. The rms baseline error of 7 cm with the six-station, two-satellite simulation was the best result obtained.

Gaposchkin and Latimer also tested another network, replacing Grand Turk with Quincy, California; Bermuda with San Diego; and Meades Ranch with Bear Lake, Utah. However, the stations are too widely separated in this configuration to obtain a sufficient number of simultaneous observations of Starlette, which is too low to be observed by more than four of these stations at once. The results of this simulation and a similar one using an eccentric Lageos orbit (5000 × 7000 km), though yielding unsatisfactory results, are displayed in Table 10.

A simulation to determine the quality of a geometrical solution based on 1 year of data is now in progress. This study includes simulated weather data.

Table 9. Errors in computed baselines for the basic network.

Case	No. of stations*	Satellite	rms error (cm)	Maximum error (cm)	Satellite positions	No. of interstation distances
1	6	Lageos, Starlette	7	13	200	15
2	6	Lageos	19	38	126	15
3	5 (minus Kansas)	Lageos, Starlette	11	23	177	10
4	5 (minus Kansas)	Lageos	33	74	126	10
5	4 (minus Kansas and Texas)	Lageos, Starlette	339	464	163	6
6	4 (minus Kansas and Texas)	Lageos	424	623	124	6

*The six stations were located in Texas, Kansas, Maryland, Florida, Bermuda, and Grand Turk.

Table 10. Errors in computed baselines for the alternative network.

Case	No. of stations*	Satellite	rms error (cm)	Maximum error (cm)	Satellite positions	No. of interstation distances
1	6	Lageos, Starlette	33	59	164	15
2	6	eccentric Lageos	66	112	174	15

*The stations used in this simulation were California (San Diego and Quincy), Utah, Texas, Maryland, and Florida.

Gaposchkin and Kalaghan have begun a simulation to support the determination of the geoid to 7 cm using the Seasat A altimetry. The eight-station network employed for the Seasat study consisted of the SAO sites in Brazil, Peru, Australia, and Hawaii plus the laser sites at GSFC, Patrick Air Force Base, MacDonald Observatory, and Meades Ranch. The error model for the Seasat simulations included the same gravity-field error as that for Lageos, and the station-position errors were random variables selected from a gaussian distribution with a zero mean and a standard deviation of 20 cm. The laser-data error consisted of two parts: a bias term, random from pass to pass, and a noise term, random from observation to observation. Both of these terms were samples from a gaussian population with zero mean and a standard deviation of 5 cm. The error in the radiation-pressure model was assumed to be a bias in the area-to-mass ratio (A/M) and was taken as

$$\delta(A/M) = 1 \times 10^{-3} \text{ cm}^2 \text{ g}^{-1} \quad .$$

Finally, the effects of weather were accounted for by randomly rejecting half the observed passes for each station. As a result of this procedure, some 1-day arcs were observed by as many as seven or as few as three stations from the eight-station network. With 4-day arcs, all stations in the network usually contributed to the total number of observations.

Preliminary results indicate that, with suitable observations, orbits can be obtained to this accuracy in the radial direction.

The network-adjustment program used for the geometrical solutions in SE III (Gaposchkin, 1973) has been modified by Latimer to include a free-net capability.

3.4 Polar Motion and Earth Rotation (RTOP 369-02-02)

This task, which is fundamental to the development of an EHA model, has an objective of measuring variations in polar motion and earth rotation to an accuracy of 1 cm over 12-hour averages. From this study, we hope to find out whether measurable correlations exist between large earthquakes and variations

in polar motion and earth rotation. Computer programs are being developed to determine pole position from satellite-tracking data. By means of a simulation program, error sources in the pole-position determination will be studied. This simulation is designed to establish the degree of sensitivity to error sources, network geometry, satellite geometry, and data volume. From these, we plan to develop theoretical models of polar motion and earth rotation. Valuable information will also be gained for more precise orbit computation, from which we will be able to determine the axis of the maximum moment of inertia of the earth from satellite-tracking data.

Geodetic station coordinates, coordinates of the earth's instantaneous pole, and polynomial coefficients of UT1 are continually being updated for analyzing recent satellite data, especially from Starlette and Geos 3.

Beginning 1 January 1975, pole coordinates of the Bureau International de l'Heure (BIH) are being used rather than those from the International Polar Motion Service (IPMS). Since the BIH coordinates are not given to the required precision, we are extrapolating them from various services, including BIH annual reports and Circulars D, IPMS, the International Latitude Service, the Naval Weapons Laboratory, and, since 12 May, the Dahlgren Polar Motion Service.

Latitude-variation data, from 1825 to the present, are being prepared on punched cards in the SAO format.

The differences between A.1 and UT1 expressed as a second-degree polynomial are currently being computed from BIH Circular D values extrapolated for a period of 1 1/2 months. We are plotting the difference between IAT and UT1 over 5-day intervals in order to derive a more reasonable extrapolation of the earth's rotation curves. Values of A.1 minus UTC are also being checked from various sources.

Geodetic station coordinates are being updated from several sources; they are being prepared in a uniform format.

Mr. Antanas Girnius is preparing a computer-accessible file of polar-motion and earth-rotation parameters and station coordinates so that the data will correspond to x, y, z values. Incorporating values for A.1 - UTC, A.1 - UT1, pole positions of the earth, and station coordinates, this work is very time consuming, as the data have accumulated over several years from many sources. The latest (6 May) coordinates of Eastern European stations have been included. Values of Δt for the period February 1962 to 4 April 1968 have been replaced with those in SE III.

3.5 Gravity Field and Tides (RTOP 369-02-03)

This task is addressed to studies of the earth's gravity field. A more detailed and more accurate model of the gravity field of the earth is needed in order to 1) place global plate-motion models on a well-constructed physical basis, 2) determine more accurate orbits for EODAP satellites, such as Lageos and Seasat A, and 3) remove geoidal undulations from altimeter data so that oceanographic features can be identified.

By analyzing surface gravimeter measurements, we can develop mean gravity anomalies with well-defined statistical properties, which can then be combined with satellite data to obtain large-scale solutions for the geopotential.

Williamson and Gaposchkin have compiled a new, combined surface-gravity data file and have incorporated these data into the Geophysical Data Base. To create this file, they added new surface-gravity data from the Defense Mapping Agency Aerospace Center (DMAAC) to the data file described in Williamson and Gaposchkin (1975), which included data from Mather (1970) and Talwani, Poppe, and Rabinowitz (1972) for regions where available, as well as data from the older DMAAC compilation (the older compilation contains measurements for some areas not included in the new one; since we believe the data are reliable, we have included them). The combined data file contains 34,384 measured means; the rms difference between this set and that described in Williamson and Gaposchkin (1975) is 15 mgal. Table 11 compares the new data set with those addressed in SE III and in Williamson and Gaposchkin (1975).

Table 11. Surface-gravity data.

Source	Number of 1° X 1° means	Number of 550-km X 550-km blocks $n \geq 1$*	Number of 550-km X 550-km blocks $n = 25$*
SE III	19,328	1183	145
Williamson and Gaposchkin (1975)	31,636	1452	485
To date	34,384	1474	539
Total possible	64,800	1654	1654

*n is the number of measurements.

A number of computer programs that process surface-gravity data and calculate the gravity field have been revised during this reporting period, and an internal report summarizing them has been written. Significant improvements have been achieved, the first of which produces a more accurate calculation of mean gravity anomalies from potential harmonic coefficients and gives an improved combination solution for the gravity field and a better calculation of the high-order coefficients determined from surface-gravity data by means of a quadrature formula. The second improvement stems from a change in the procedure that obtains combination solutions. As a result, more coefficients can be calculated from the surface-gravity data. Specifically, we can now determine all tesseral-harmonic coefficients with $\ell \leq 36$. Williamson has prepared the documentation for these revised computer programs.

Since the determination of the SE III gravity field, a revised gravity field has been calculated by Gaposchkin, Williamson, and Ms. Gerry Mendes by using the improved programs, the new data, and the satellite normal equations from SE III. In an effort to select the best reference field, Gaposchkin and Williamson compared the SE III solution with three new gravity-field combination solutions (called T2, T3, and T4) based on the surface-gravity data described in Williamson and Gaposchkin (1975) and on the revised computer programs. Table 12 summarizes the contents of the combination solutions, and Table 13 compares the solutions with each other.

The following quantities, defined by Kaula (1966), are computed and shown in Table 13:

$\langle g_t^2 \rangle$ The mean value of g_t^2, where g_t is the mean free-air gravity anomaly based on surface gravity, indicating the amount of information contained in the surface-gravity anomalies.

$\langle g_s^2 \rangle$ The mean value of g_s^2, where g_s is the mean free-air gravity anomaly computed from the geopotential model, indicating the amount of information in the computed gravity anomalies.

Table 12. Summary of combination solutions for the gravity field.

Solution	Anomalies used	Calculated mean gravity anomaly	Gravity-data normals	Unmeasured regions
SE III	1183	old	$18 \geq \ell \geq 9$	reference field
T2	1452	new	$18 \geq \ell \geq 9$	ellipsoid
T3	1452	new	$18 \geq \ell \geq 1$	ellipsoid
T4	1452	new	$18 \geq \ell \geq 1$	reference field

Table 13. Comparison of combination solution with surface gravity (in $mgal^2$).

Solution	Anomalies used		$\langle g_s^2 \rangle$	$\langle g_t^2 \rangle$	$\langle g_t g_s \rangle$	D	$\langle (g_t - g_s)^2 \rangle$	$E(\epsilon_s^2)$	$E(\epsilon_t^2)$	$E(\delta g^2)$
	old									
SE III $\ell \leq 18$	$n \geq 1$	1183	258	302	202	237	156	56	24	75
	$n \geq 20$	306	236	311	221	237	105	15	13	77
	new									
SE III $\ell \leq 18$	$n \geq 1$	1452	244	309	177	235	199	67	19	113
	$n \geq 20$	678	267	356	243	235	138	24	15	98
	new									
SE III* $\ell \leq 18$	$n \geq 1$	1452	230	309	172	235	193	57	19	118
	$n \geq 20$	678	254	356	237	235	135	16	15	104
	new									
T2* $\ell \leq 18$	$n \geq 1$	1452	225	309	190	223	155	35	19	100
	$n \geq 20$	678	260	356	252	223	111	7	15	89
	new									
T3* $\ell \leq 18$	$n \geq 1$	1452	209	309	193	209	130	15	19	97
	$n \geq 20$	678	241	356	253	209	91	-12	15	88
	new									
T4* $\ell \leq 18$	$n \geq 1$	1452	211	309	194	214	132	17	19	96
	$n \geq 20$	678	241	356	253	214	91	-12	15	88

* Based on the improved formula for calculated gravity anomalies.

$\langle g_t g_s \rangle$ An estimate of g_h — i.e., the true value of the contribution to the gravity anomaly of the geopotential model and the amount of information common to both g_t and g_s.

$\langle (g_t - g_s)^2 \rangle$ The mean square difference of g_t and g_s.

$E(\varepsilon_s^2)$ The mean square error in the geopotential model.

$E(\varepsilon_t^2)$ The mean square error of the observed gravity.

$E(\delta g^2)$ The mean square of the error of omission — that is, the difference between true gravity and g_h; this term is then the model error.

If the geopotential model were perfect, then $\langle g_s^2 \rangle = \langle g_h^2 \rangle$, which in turn would equal $\langle g_t g_s \rangle$ if g_t were free from error and known everywhere. Then, ε_s^2 would be zero even though g_s would not contain all the information necessary to describe the total field. The information not contained in the model field — i.e., the error of omission, δ_g — then consists of the higher order coefficients. The quantity $\langle (g_t - g_s)^2 \rangle$ is a measure of the agreement between the two estimates g_t and g_s and is equal to

$$\langle (g_t - g_s)^2 \rangle = E(\varepsilon_s^2) + E(\varepsilon_t^2) + E(\delta g^2) \quad .$$

Another estimate of g_h can be obtained from the gravimetric estimates of degree variance σ_ℓ^2 (Kaula, 1966):

$$E(g_h^2) = D = \sum_\ell \frac{n_\ell}{2\ell + 1} \sigma_\ell^2 \quad ,$$

where n_ℓ is the number of coefficients of degree ℓ included in g_h, and

$$\sigma_\ell^2 = \gamma^2 (\ell - 1)^2 \sum_m \left(\bar{C}_{\ell m}^2 + \bar{S}_{\ell m}^2 \right) .$$

We also have

$$E(\varepsilon_s^2) = \langle g_s^2 \rangle - \langle g_s g_t \rangle$$

and

$$E(\varepsilon_t^2) = \langle g_t^2 \rangle / \langle n \rangle \quad .$$

Of particular interest in Table 13 is the reduced amount of information in the computed gravity anomalies ($\langle g_s^2 \rangle$) and the small difference between solutions T3 and T4. Because of this small difference, we feel that the areas where we have no surface-gravity measurements may have a less significant effect on the new solution than on previous solutions; this is probably because of the increase in the number of measured areas. From the new combination solutions, higher order gravity-field coefficients have been calculated from an iterative procedure that uses a quadrature formula to calculate corrections to the coefficients. Satellite orbits have also been calculated with the new solution, with weights assigned to the surface-gravity data being varied. These results are summarized in Table 14. Nevertheless, the new solutions do not supply uniform improvement over the SE III solution. Therefore, we have decided to use SE III as the initial reference field for the determination of our new Standard Earth.

This new determination of the gravity field has been started. We have selected five arcs for each of five satellites: Geos 1, BE-C, Geos 2, Starlette, and Peole. We will obtain a series of solutions by combining the surface-gravity normal equations with a combination of 1 to 5 of the satellite normal equations; Geos 3 may be added as a sixth satellite when the data become available. We are studying what effects might result to the solution if we increase the number of satellites. In addition, we will include 25 arcs of data taken during the ISAGEX campaign.

3.6 Ground Systems Requirements and Plans (RTOP 639-01-03)

Satellite determination of plate motion will depend on the position and selection of sites comprising the fundamental EODAP network. Of major concern in this selection are geological, geophysical, and operational considerations associated with each laser tracking site. Also relevant are the political and environmental conditions conducive to long-term operations.

Mohr and Mao have nearly completed a preliminary evaluation, based on published works, summarizing data regarding the geology, plate tectonics,

Table 14. Satellite orbits calculated with different weights. The epoch is listed under the satellite name; σ is the standard error of unit weight, and N is the number of observations.

Solution	Weight	Geos 1 41574 σ	N	Geos 2 41573 σ	N	Peole 41792 σ	N	BE-C 41564 σ	N	Starlette 42496 σ	N
SE III	w*	3.31	721	5.41	209	—	—	2.74	197	5.96	336
T3	w/10	4.22	725	7.50	209	7.82	218	—	—	—	—
T3	w/4	3.60	723	4.62	209	7.08	216	3.08	197	4.52	326
T3	w	3.85	713	4.14	209	7.60	195	3.24	197	—	—
T3	w × 4	4.53	720	3.17	209	9.35	222	3.27	197	4.16	321
T3	w × 10	6.35	731	3.48	197	9.43	222	—	—	—	—

* w = the weight used in SE III.

crustal deformation, and seismicity for 26 existing or proposed laser stations, identified in Table 15 and shown in Figure 7. Also shown in Figure 7 are the relative motions of plates and earthquake epicenters. The chosen sites are scattered over the globe such that every major plate, with the exception of Antarctica, carries at least one. In selecting the locations, they gave preference to shield areas that have been stable since the early history of the earth (> 2 G.y.). Other favorable criteria include remoteness from active plate margins or intraplate deformation zones and from recently glaciated areas and coastal margins. The station sites have been classified in a simple scheme incorporating strain-accumulation and strain-release (earthquake) risks.

Important for evaluative purposes are the geological and seismological maps that accompany each site description. Reflected on these are, for example, 1) historical seismicity and tectonics, 2) young volcanic structures, where present, 3) old Precambrian grain of the earth's crust, where relevant, and 4) effects of Pleistocene glaciation, in terms of isostasy.

The report discloses that 15 of the 26 sites qualify as stable stations whose motions are likely to reflect only gross plate motion. The others, including two of the present laser station sites, fail to qualify unless additional monitoring schemes can be included, such as precise geodetic surveying of ground deformation.

We plan to distribute this report as an SAO Special Report during the next fiscal year. The finished document will also include summary operational and cloud-cover data for the 26 sites.

3.7 Analytical Models of Earth Motion (RTOP 161-02-07)

By using gross earth data, a complete strain field for the earth's interior can be computed. Some of the data to be incorporated will include geopotential and seismic travel times and detailed surface measurements. EHA

Table 15. Locations of stations shown in Figure 7.

Station number	Station location	Station number	Station location
1	Argentina, Comodoro Rivadavia	14	Japan, Tokyo
2	Atlantic Ocean, Bermuda	15	Korea, Pusan
3	Australia, Orroral Valley	16	Pacific Ocean, Rapa Nui
4	Brazil, Natal	17	Pacific Ocean, Guam
5	Brazil, Porto Alegre	18	Pacific Ocean, Maui, Hawaii
6	Brazil, São Francisco	19	Pacific Ocean, Tutuila, Samoa
7	Canada, Fort Resolution	20	Pacific Ocean, Tahiti
8	Ecuador, Quito	21	Pacific Ocean, Wake Island
9	Egypt, Cairo	22	Peru, Arequipa
10	Ethiopia, Debre Zeit	23	Spain, San Fernando
11	Greece, Athens	24	Sweden, Uppsala
12	India, Bangalore	25	Thailand, Bangkok
13	India, Naini Tal	26	USA, Mt. Hopkins, Arizona

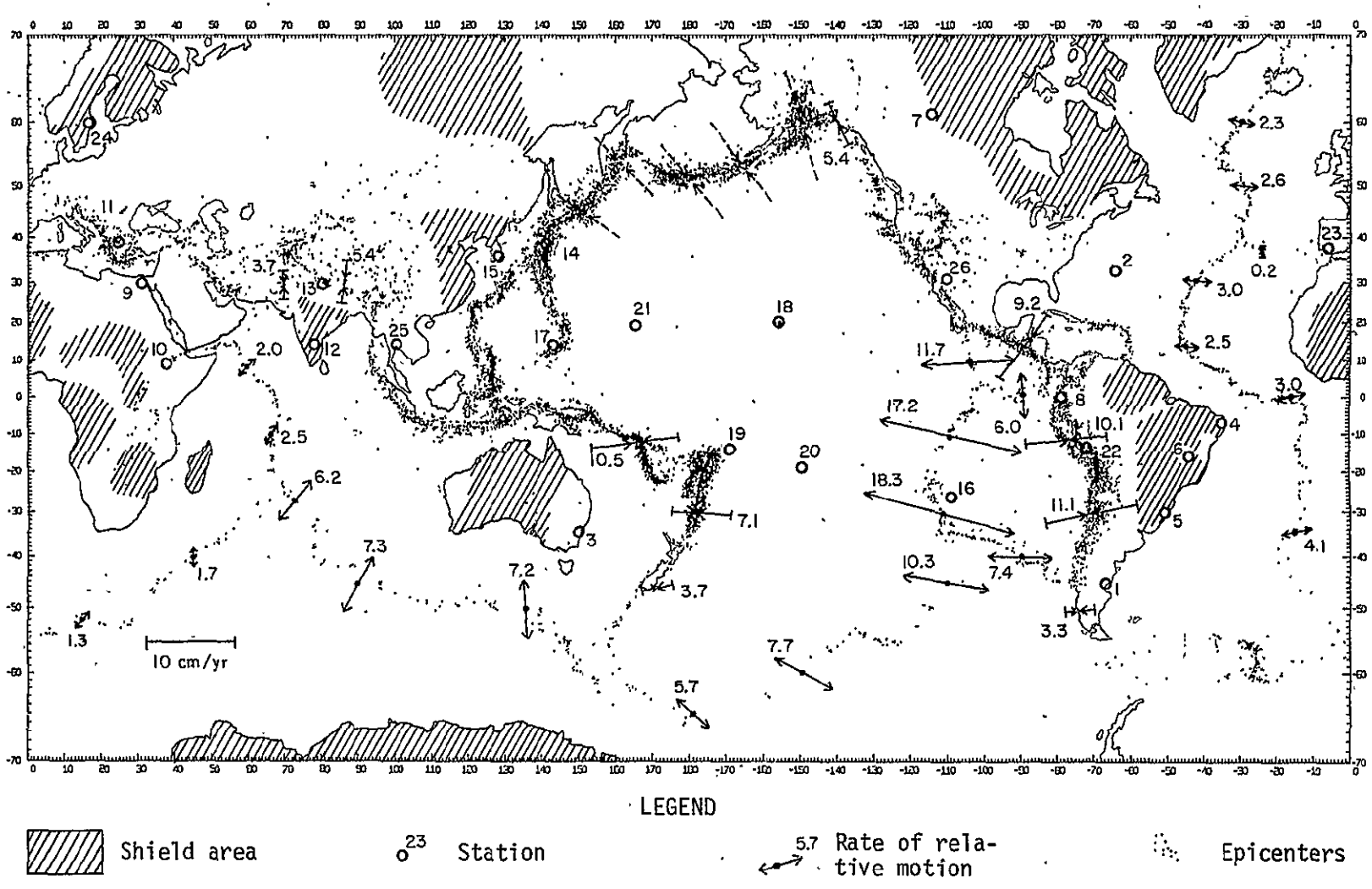

Figure 7. World map showing station locations, earthquake epicenters for the period 1961 through 1967 (after Barazangi and Dorman, 1969), and relative motions of plates (after Minster et al., 1974, model RM1).

models will be developed through computer programs to convert these and other data into predictions of probable times, locations, and magnitudes of earthquakes.

Within the scope of this task, a basic mathematical model for earth strain, including the dependence on observables, will be developed. For solving the required system of partial-differential equations, numerical methods will be studied and preliminary computer programs designed. We will also establish overall computer requirements for a general solution when sufficient data become available.

The data collected for this task will also be used to define unstable areas and, in combination with other data, to gain more understanding of gravity anomalies.

The large-scale deformation field will be formulated in spherical coordinates. The formulation will include elastic and viscous parameters, with boundary data specified in terms of spherical harmonics (e.g., the geopotential) and detailed geographical data within the Geophysical Data Base. The solution will be obtained by numerical integration of partial-differential equations.

3.8 Laser Techniques (RTOP 639-05-02)

3.8.1 Retroreflector-array transfer functions

A report giving the transfer function of the Starlette retroreflector array was published in February. A summary of the results is included in the section entitled "Geometrical Transfer Function of the Retroreflector Array" on page 10 of the CNES document "Starlette" dated February 1975. The analysis shows range errors introduced by the spacecraft to be less than 0.5 cm. Experimentally measured return-signal strengths from Starlette indicate that the spherical retroreflector-array configuration gives measurable returns at altitude angles below 20°, as indicated by the analysis.

The transfer function of the Geos 3 retroreflector array has been computed, and the report will be published in July. Figure 8 gives the range correction as a function of the angle of incidence of the laser beam. Special attention has been given to the difference between the range corrections for the pulse centroid, the half-maximum, and the half-area detection methods and between the coherent and the incoherent range corrections for these same methods. Some new computational procedures have been developed, such as the use of reflectivity curves for specific wavelengths and velocity aberrations and the computation of pulse shapes at specific points in the far field. Contour plots are employed to show intensity and range variations in the far field. A sample range contour plot is shown in Figure 9. The 45° tilt of the cube-corner array results in large reflectivity at low satellite elevation angles, as shown in Figure 10. The experimental data show that the spacecraft gives strong returns close to the horizon, as indicated by the analysis.

A transfer function has also been computed for the infrared cube corner carried by Geos 3. Figure 11 shows the reflectivity of the cube as a function of incidence angle and polarization of the transmitted laser beam. Since the spacecraft is triaxially stabilized, infrared observations can be accurately related to the satellite's center of gravity.

Simulations have been conducted to evaluate the effect of the range correction of variations in the performance of an array with cube corners of different reflectivities. In a worst-case simulation, the effect of a 3-db variation was within the 5-mm accuracy requirement for Lageos.

A design study was carried out on the proposed infrared cube-corner array for Lageos. Hollow, Irtran-2, and germanium cube corners in two- and six-cube configurations were analyzed to see what configuration gives the highest probability of getting a return without having interference between reflections from different cubes. We found the highest probability to be from two solid-germanium cubes. If the satellite is gravity stabilized with the cube corners

PHI (DEG)	RANGE CORRECTION (METERS)
0.0	1.3043
1.0	1.3047
2.0	1.3059
3.0	1.3080
4.0	1.3108
5.0	1.3145
6.0	1.3186
7.0	1.3231
8.0	1.3279
9.0	1.3328
10.0	1.3380
11.0	1.3431
12.0	1.3478
13.0	1.3523
14.0	1.3563
15.0	1.3599
16.0	1.3630
17.0	1.3656
18.0	1.3676
19.0	1.3691
20.0	1.3701
21.0	1.3707
22.0	1.3713
23.0	1.3716
24.0	1.3715
25.0	1.3709
26.0	1.3699
27.0	1.3684
28.0	1.3666
29.0	1.3643
30.0	1.3616
31.0	1.3585
32.0	1.3549
33.0	1.3508
34.0	1.3462
35.0	1.3411
36.0	1.3356
37.0	1.3297
38.0	1.3235
39.0	1.3168
40.0	1.3097
41.0	1.3022
42.0	1.2942
43.0	1.2858
44.0	1.2769
45.0	1.2676
46.0	1.2577
47.0	1.2473
48.0	1.2365
49.0	1.2253
50.0	1.2137
51.0	1.2017
52.0	1.1894
53.0	1.1767
54.0	1.1637
55.0	1.1504

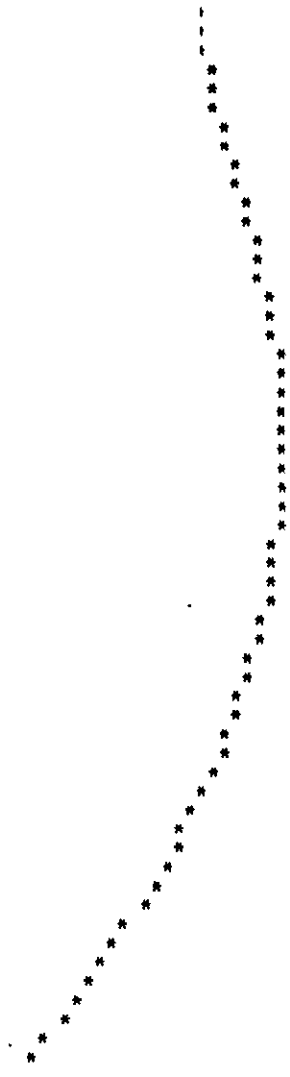

Figure 8. Average centroid range correction in the 25- to 50-μrad annulus of the far-field pattern versus incidence angle, λ = 6943 Å.

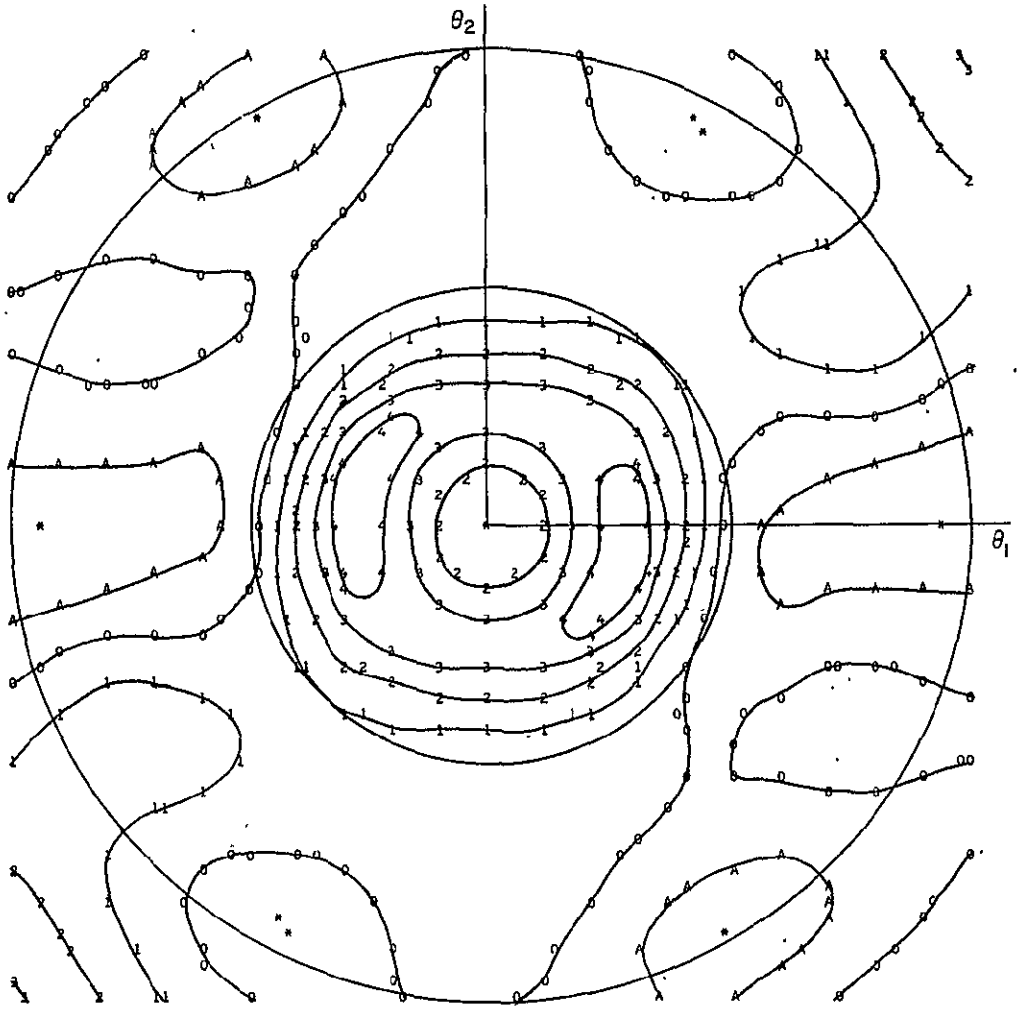

Figure 9. Contour plot of a centroid range-correction matrix. Circles of radius 25 and 50 μrad are shown to mark the minimum and maximum values of the velocity aberration. On the plot, the symbol A indicates that the range correction minus the average range correction in the 25- to 50-μrad annulus is equal to +1 cm; 0 equals 0 cm; and 1 through 4 equal -1 through -4 cm. $\phi = 45°$, $\delta = 2\overset{\circ}{.}0$, $\lambda = 6943$ Å.

PHI (DEG)	REFLECTIVITY
0.0	13.8152
1.0	13.9392
2.0	14.0522
3.0	14.1542
4.0	14.2451
5.0	14.3247
6.0	14.5429
7.0	14.8489
8.0	15.2425
9.0	15.7016
10.0	16.1949
11.0	16.9008
12.0	17.7405
13.0	18.6415
14.0	19.5677
15.0	20.4991
16.0	21.5805
17.0	22.7439
18.0	23.9256
19.0	25.1052
20.0	26.2602
21.0	27.4096
22.0	28.4329
23.0	29.4027
24.0	30.3372
25.0	31.2489
26.0	32.1222
27.0	32.9793
28.0	33.7877
29.0	34.5745
30.0	35.3561
31.0	36.1214
32.0	36.8676
33.0	37.5906
34.0	38.3623
35.0	39.1284
36.0	39.8863
37.0	40.6168
38.0	41.2922
39.0	41.7810
40.0	42.1089
41.0	42.2956
42.0	42.3424
43.0	42.3173
44.0	42.1546
45.0	41.8672
46.0	41.4072
47.0	40.8101
48.0	40.0850
49.0	39.2887
50.0	38.4285
51.0	37.5242
52.0	36.5497
53.0	35.5040
54.0	34.4152
55.0	33.2708

ONE REFLECTOR AT NORMAL INCIDENCE HAS UNIT REFLECTIVITY

PHI (DEG)	REFLECTIVITY
56.0	32.0954
57.0	30.8587
58.0	29.5680
59.0	28.2297
60.0	26.8592
61.0	25.4667
62.0	24.0744
63.0	22.6834
64.0	21.3307
65.0	20.0170
66.0	18.7418
67.0	17.5065
68.0	16.3334
69.0	15.2342
70.0	14.2083
71.0	13.2635
72.0	12.3609
73.0	11.4964
74.0	10.6758
75.0	9.9117
76.0	9.2262
77.0	8.5509
78.0	7.8838
79.0	7.2348
80.0	6.6082
81.0	6.0407
82.0	5.4752
83.0	4.9132
84.0	4.3711
85.0	3.8538
86.0	3.3732
87.0	2.9162
88.0	2.4837
89.0	2.0873
90.0	1.7383
91.0	1.4347
92.0	1.1591
93.0	.9166
94.0	.7086
95.0	.5469
96.0	.4261
97.0	.3185
98.0	.2289
99.0	.1543
100.0	.1049
101.0	.0813
102.0	.0583
103.0	.0368
104.0	.0176
105.0	.0055
106.0	.0044
107.0	.0033
108.0	.0021
109.0	.0010

ONE REFLECTOR AT NORMAL INCIDENCE HAS UNIT REFLECTIVITY

Figure 10. Average reflectivity of the Geos 3 optical retroreflector array in the 25- to 50-μrad annulus of the far-field diffraction pattern, λ = 6943 Å.

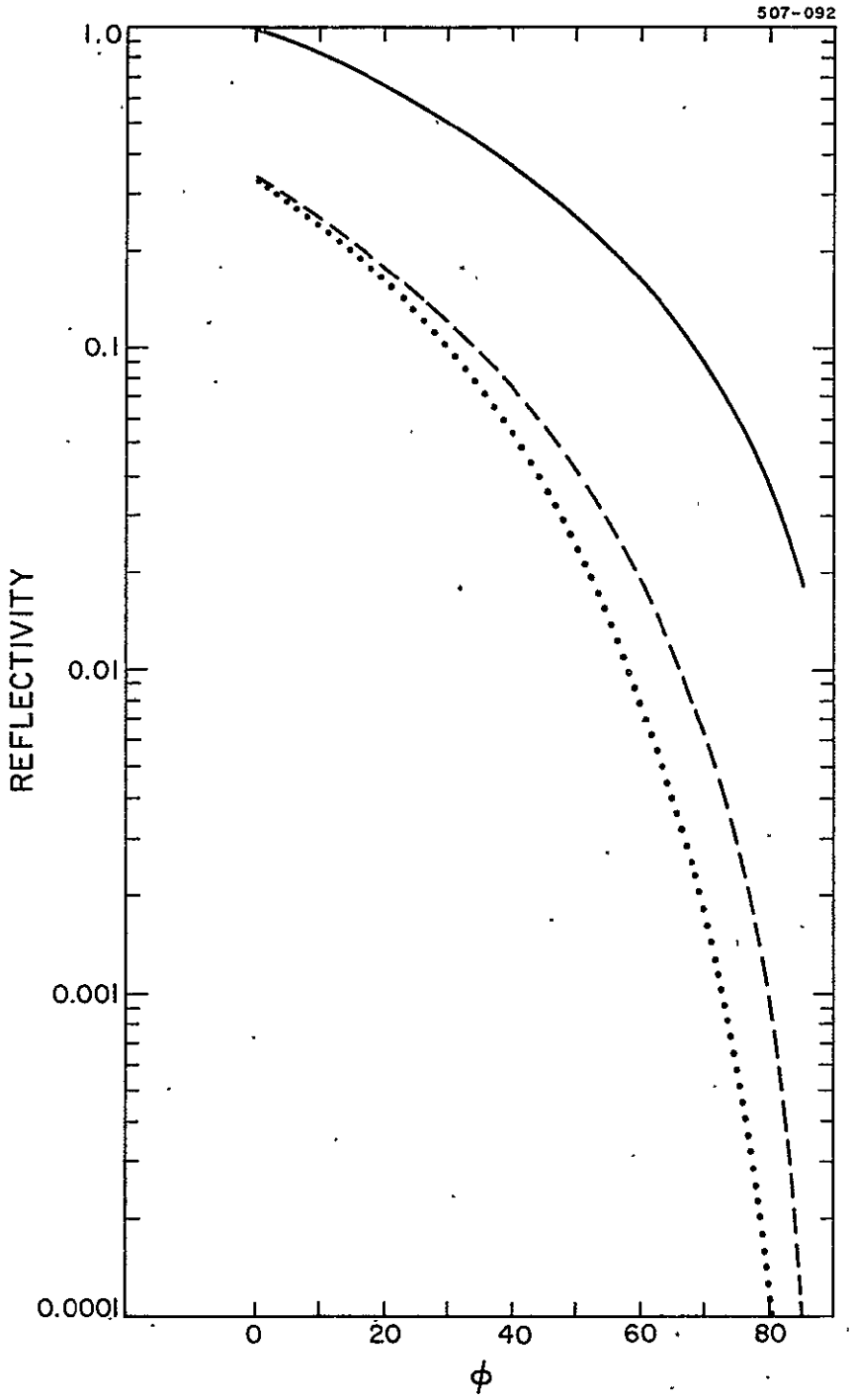

Figure 11. Active reflecting area (solid curve) and average reflectivity in the 25- to 50-μrad annulus of the far-field diffraction pattern for the Geos 3 infrared reflector. The dashed and dotted curves represent the electric field vector $\vec{E}$ parallel and perpendicular, respectively, to the plane of incidence. $\theta = 30°$, $n = 2.19$, $\lambda = 10600$ Å.

on opposite poles of the axis of stabilization, a continuous return signal will result that can be accurately related to the center of the spacecraft. Figure 12 shows the reflectivity of the germanium cubes versus incidence angle.

Baker-Nunn camera visibilities have been computed for Lageos for various launch times; the best ones were obtained for a launch window from midnight to 4 AM or noon to 4 PM. Because of thermal considerations, a launch window from 11 PM to 2 AM was chosen by NASA. Baker-Nunn and radar tracking of Lageos has been discussed with the Delta Program Office at Goddard. SAO has arranged for the U. S. Air Force to provide radar tracking of Lageos during the acquisition period.

New equations have been derived for the diffraction analysis of triangular and hexagonal retroreflectors and have been put into the retroreflector-array computer programs. The draft of an SAO Special Report documenting the analytic technique for computing transfer functions is being revised and updated. The current plan is to submit this for publication in early FY 1976.

With the completion of the Starlette and Geos 3 transfer functions, no continuation of this task has been requested in FY 1976.

3.8.2 Systems analysis — Simulations

The Experimental Geophysics Department provided support to the Analytical Satellite Geophysics Department in the development and application of systems simulation software. This support included the development of weather and system performance models and their implementation into the simulation software.

In FY 1976, the systems simulations will be carried out under other task areas. No continuation of this task has been requested.

3.8.3 Systems analysis — Instrumentation

An upper bound for the short-term stability of the new pulse-processing system has been estimated by comparing calibration values before and after

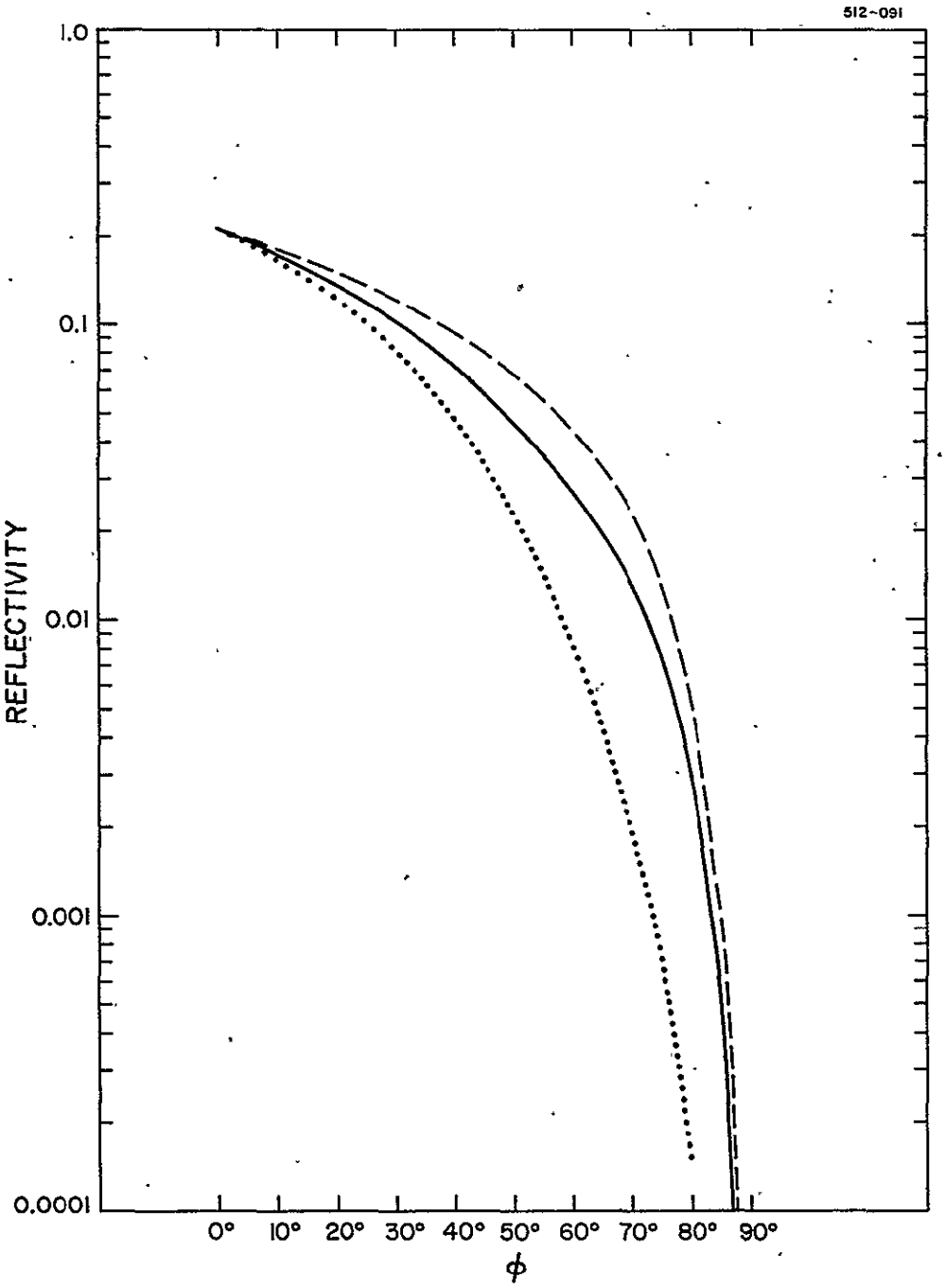

Figure 12. Average reflectivity of a Lageos infrared cube corner in the 32- to 41-μrad annulus of the far-field diffraction pattern, λ = 10600 Å. The dashed and dotted curves represent the electric field vector $\vec{E}$ parallel and perpendicular, respectively, to the plane of incidence. The solid curve represents circular polarization.

satellite transits. Figure 13 shows the difference between these calibrations, both made at approximately the same signal level during May. The standard deviation of the "before - after" differences for this period was about 1.3 nsec.

Extensive data were taken over the 6-month period to obtain an empirical expression for ranging-system calibration. It is essential that this calibration be valid over a dynamic operating range of 30 db (1 to 1000 photoelectrons per pulse). Analysis of these data shows that the calibration at Mt. Hopkins varies with signal strength above 400 photoelectrons.

A very large number of data points is needed to determine the calibration expression with acceptable precision. At low signal strengths, the expression is constant but the random error of a single point is large. Hence, many points must be averaged to reduce this error significantly. At high signal strengths, the random error is small but the calibration varies with signal strength. In this case, many points are needed to make an empirical determination of the calibration expression's variation with signal strength. Our approach was to take the maximum practical amount of data in order to reduce the random errors.

Figure 14 shows averaged data resulting from two calibration runs (1000 pulses each) on the same day. For points below 25 photoelectrons (indicated by dots), large random errors are associated with the finite data samples. Above 25 photoelectrons, where the points are represented by crosses, the random errors are small and the positions of the points are nearly independent of sample size. It is here that we can take the dispersion among the points as a measure of the system error. This is done by using linear regression to establish a best-fitting line and then finding the residual of the points from the line. The residual came out to be 0.7 nsec for Figure 14. The residuals from four other similar calibrations, run on different days, were between 0.6 and 1.4 nsec.

Figure 15 shows the combined results of all single-day calibrations over a 3-month period. The residual calculated from these data is 1.8 nsec (or 27 cm). This measured value represents an upper bound to the error introduced by the

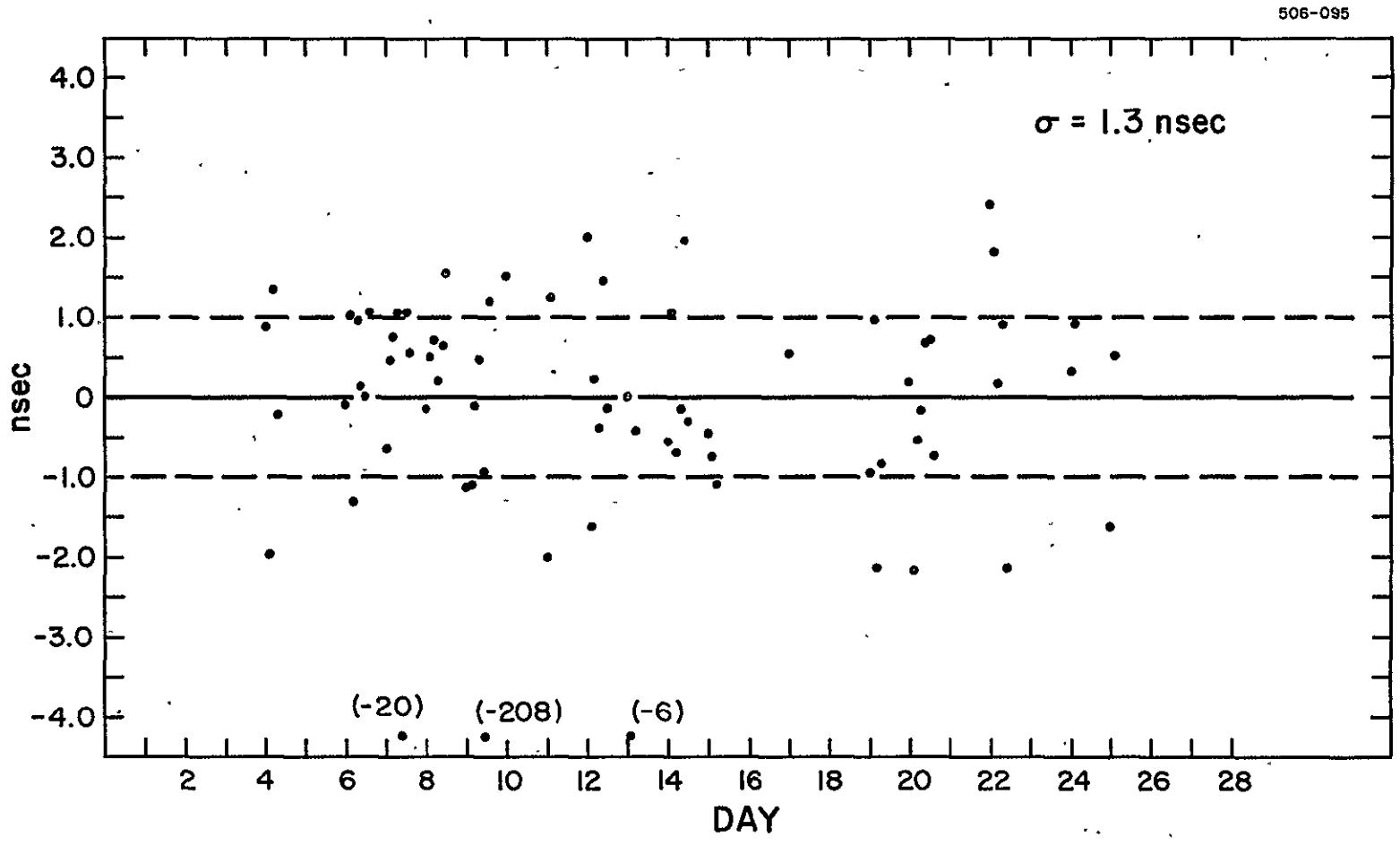

Figure 13. Calibration stability at Mt. Hopkins (precalibration minus postcalibration).

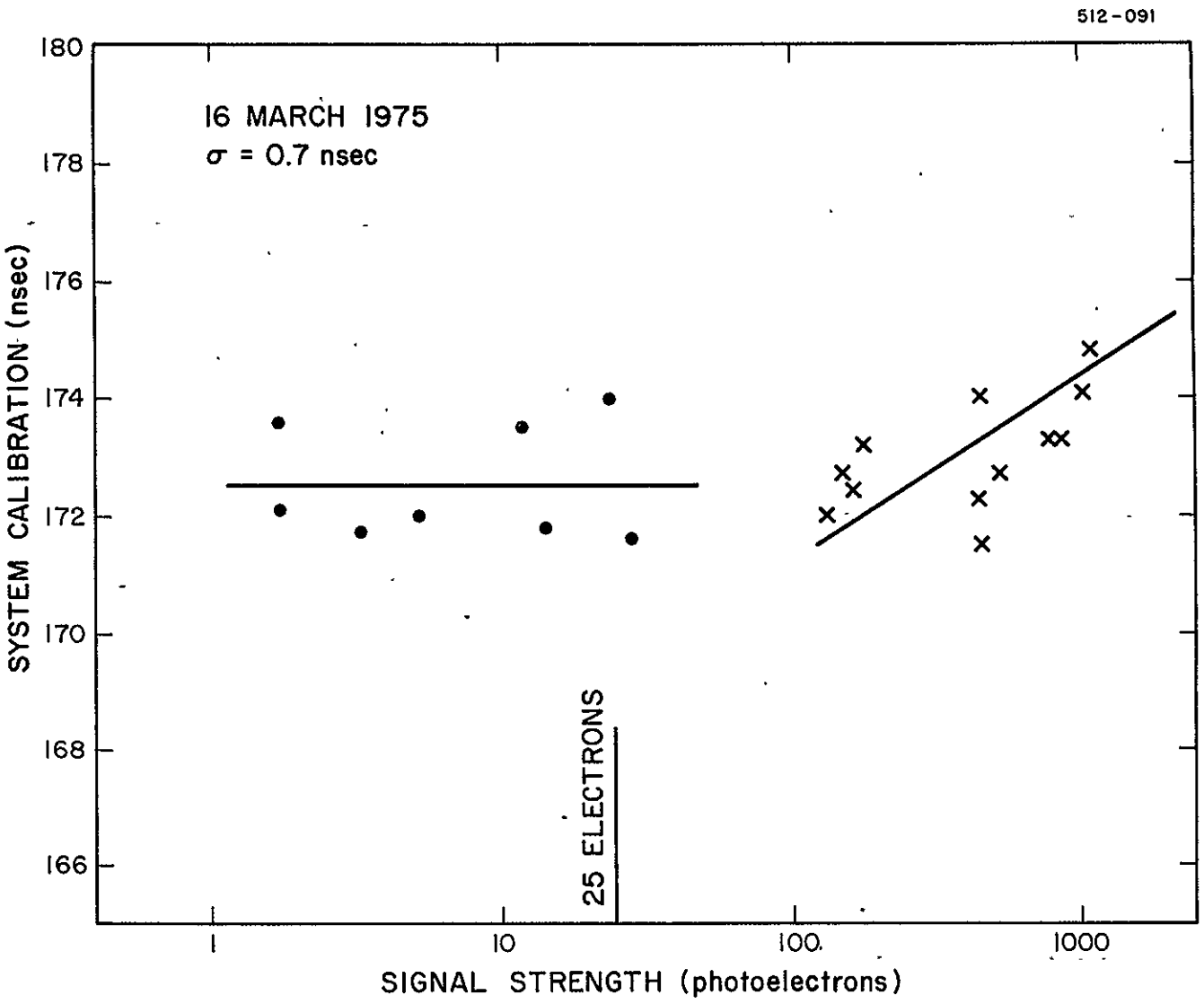

Figure 14. Calibration data taken on a single day (2000 calibration pulses).

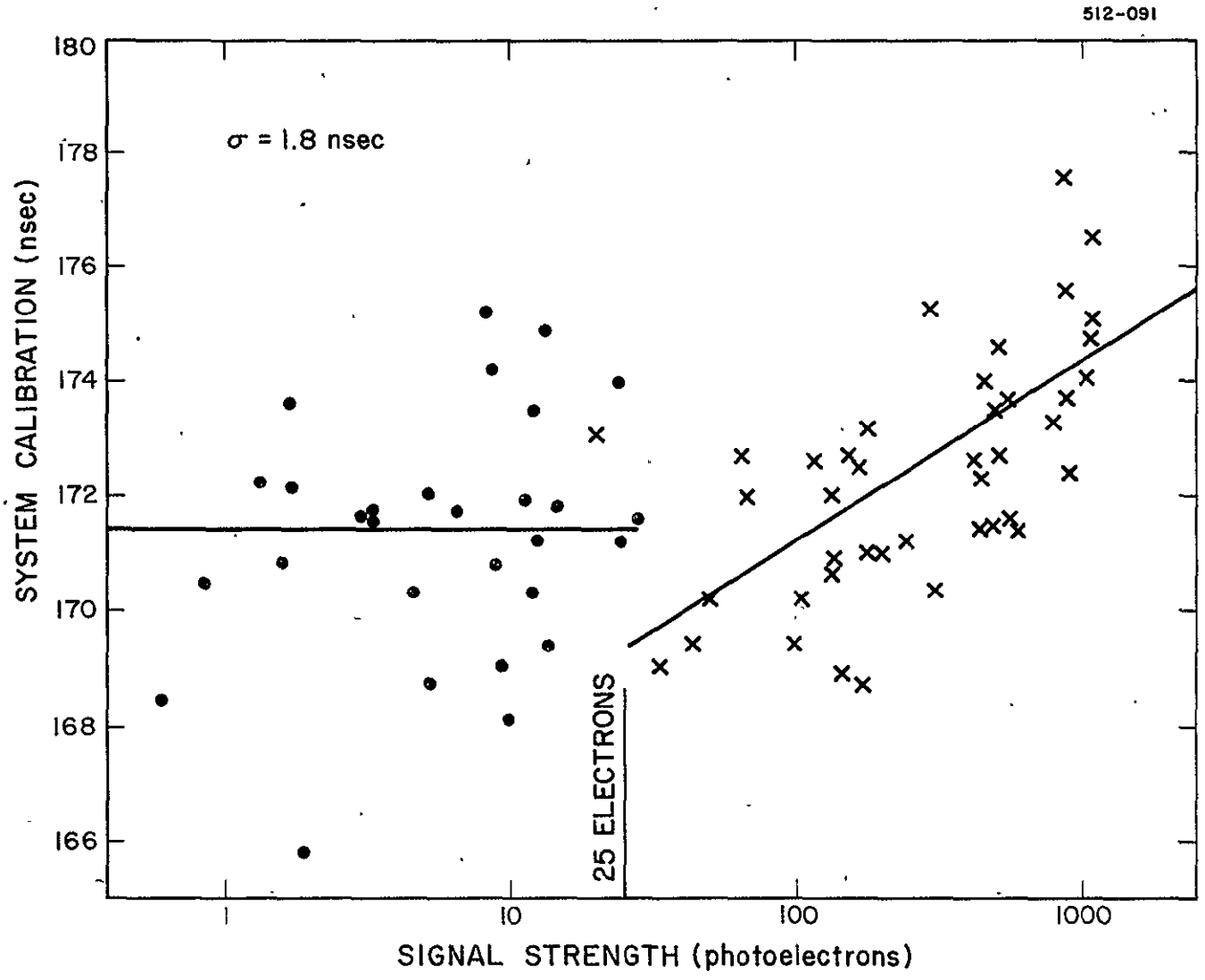

Figure 15. Composite results of 7000 calibration pulses obtained between 16 March and 7 June 1975.

digitizing electronics. It may be possible to reduce it somewhat by finding a fit to the data that is better than a straight line and by adjusting the calibration for day-to-day variations.

The signal loss that had been found earlier was also observed after the digitzer was installed. The large numbers of new data showed that this loss is not constant but, instead, varies with signal level and from day to day (see Figure 16).

Locating the source of this signal loss is difficult because absolute radiometric measurements, although they need be made at only one wavelength, must cover a range of 170 db, the ratio of the transmitted to the received energy. Our approach during the period of this report was to introduce new techniques and to make the following special measurements:

A. A new calibration of the pulse digitizer was made by applying Poisson statistics to series of very low-level returns.

B. Photon counting was introduced as a means of checking receiver efficiency.

C. Two radiometers, borrowed from EG&G, Inc., were employed to obtain measurements of energy and power that are independent of our other calibrations.

Figure 17 relates these measurements to a block diagram of the system.

We found that the new calibration of the pulse digitizer confirmed our previous value. Photon counting gave the same value of receiver efficiency as did our previous, more complicated method, based on oscilloscope photographs. The results from the first EG&G radiometer (see Figure 18) confirmed the validity of our calorimetric measurements of laser output energy and also showed that there was no significant loss in the transmitting telescope. The second EG&G radiometer gave results that were inconsistent with our receiver-efficiency measurements and with the manufacturer's value for the quantum

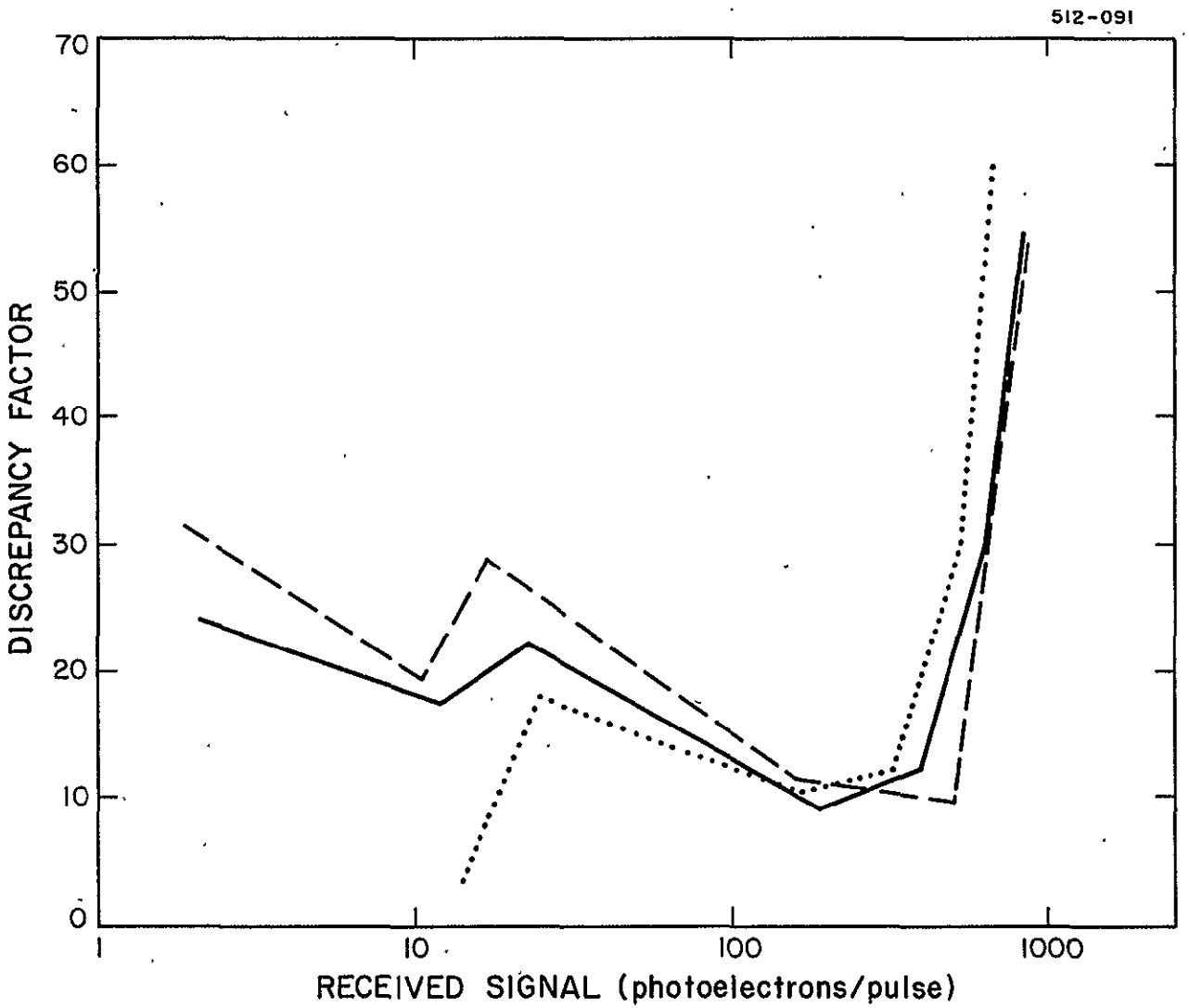

Figure 16. Signal-loss variation with strength of received signal (the three lines represent the results obtained on three different days).

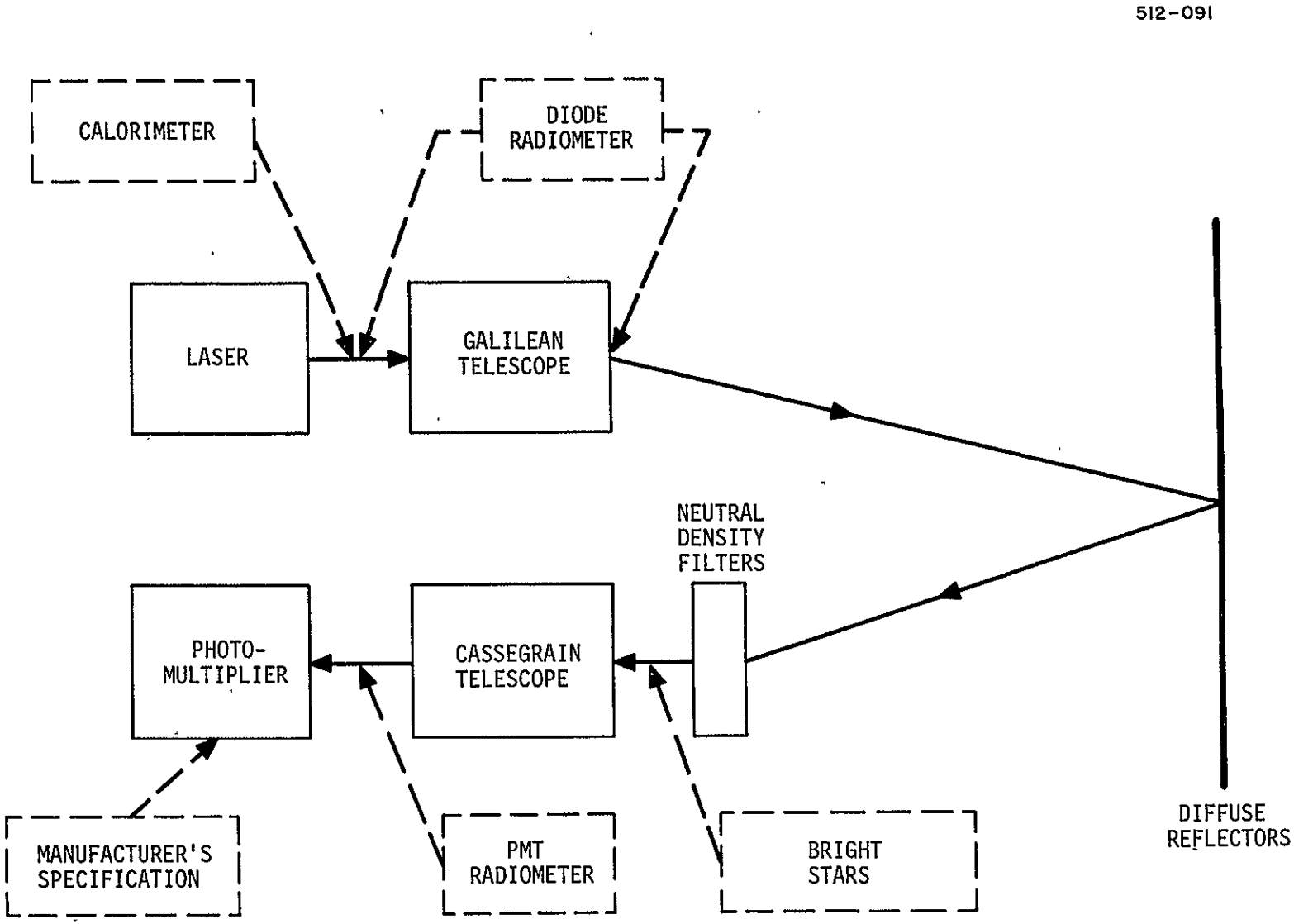

Figure 17. Radiometric measurements.

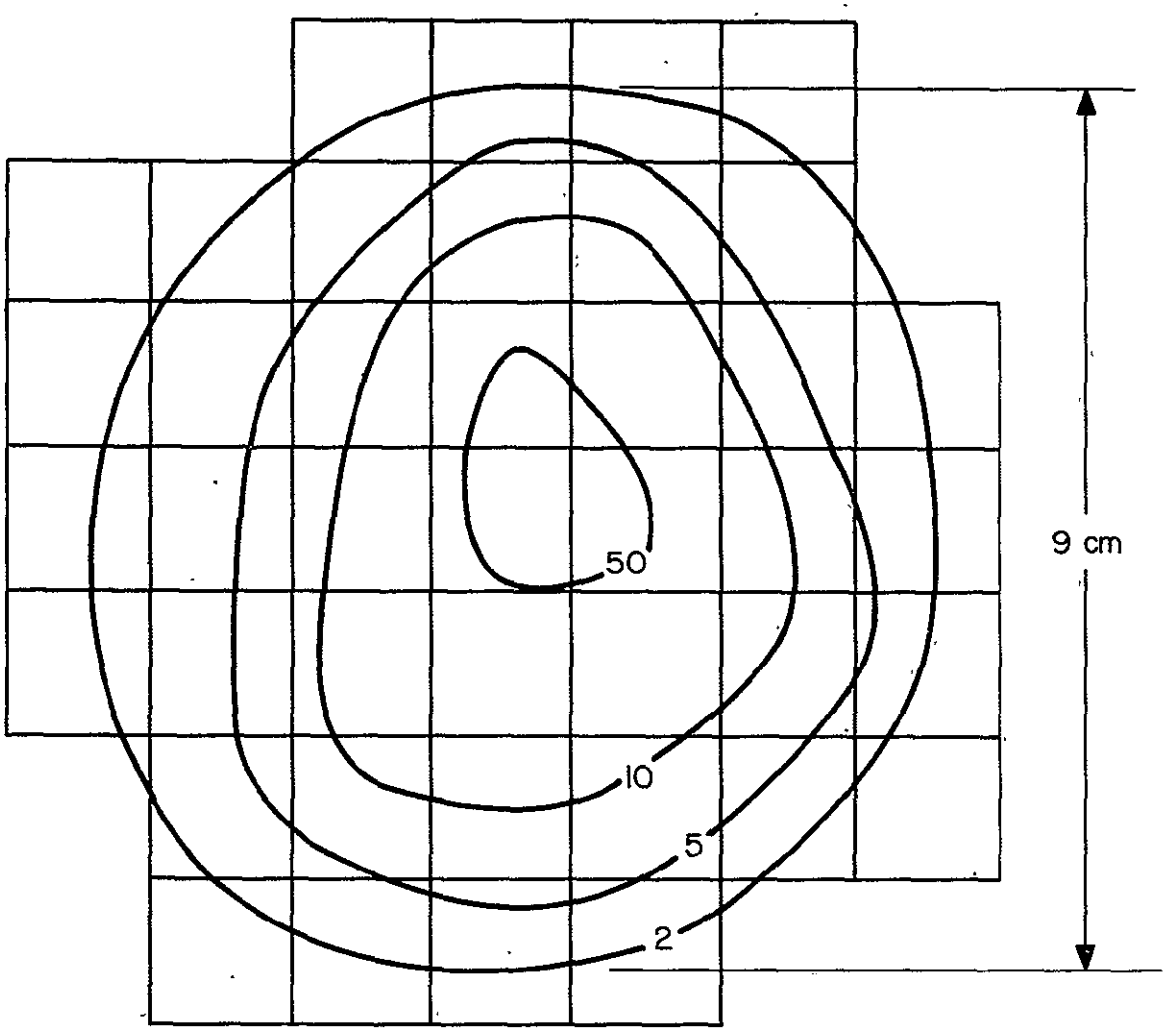

Figure 18. Profile of transmitted beam (energy densities in mJ cm^{-2}).

efficiency of the photomultiplier tube. Part of the problem was that the EG&G instrument integrated scattered light from the atmosphere into the laser returns that came from the target. Its pulsed-mode operation also turned out to be less reliable in the field than in the laboratory. Additionally, measurements had to be made at the instrument's lowest range, where the probability of error is greatest.

Further measurements of received energy and power will be made to resolve the inconsistency. We plan to have one of our own photomultipliers calibrated by a standards laboratory, to replace our gelatin neutral-density filters with calibrated glass filters, and to use more sophisticated equipment for photon counting.

3.9 Orbit-Computation Techniques (RTOP 161-05-05)

With an objective of developing an algorithm for computing satellite ephemerides with an accuracy of 1 cm, this study encompasses several tasks, including gravitational and radiation-pressure perturbations, reference systems, and development of minicomputer software for field stations. Precise orbit computation is fundamental to all satellite techniques in EODAP.

3.9.1 Gravitational perturbations

Complete expressions for zonal-harmonics perturbations expressed in terms of Hill variables (Aksnes' theory) and Delaunay variables (Kozai and Gaposchkin's theory) are being developed for comparison and verification with each other. Currently, the precision orbit-computation program utilizes combined expressions from the two theories. Dr. Kaare Aksnes expresses the long-period perturbations in terms of the Hill variables, while Dr. Hiroshi Kinoshita is calculating the long-period perturbations in terms of the Delaunay variables in order to derive expressions for the most important third-order perturbations.

The third-order periodic perturbations and the fourth-order secular perturbations are being derived by the Lie-Hori method. The gravitational potential includes the second, third, and fourth zonal harmonics. In this theory, all quantities are developed into power series of the eccentricity, but the solution is obtained in closed form with respect to the inclination. The accuracy that we hope to achieve is 1 cm. A determining function that eliminates the short-period terms S_1, S_2, and S_3 and the long-period terms S_1^*, S_2^*, S_3^* has already been obtained.

The final formulas of the periodic perturbations are expressed in terms of $L = (\mu a)^{1/2}$, e cos g, e sin g, $\ell + g$, and h, which are not singular at zero eccentricity. Position and velocity can be derived from these elements. These same determining functions have also been obtained by use of the department's computer algebra program. This theory is being compared with the current second-order theory and with numerical integration.

Dr. Yoshihide Kozai's theory for the long-period perturbations due to zonal harmonics neglects terms with the argument $i \times \omega$, the argument of perigee, where $i \geq 4$. Kinoshita has calculated these neglected perturbations, for which the order of magnitude is found to be about 4 m for Geos 1.

Expressions have been derived for some incomplete terms in the Kaula theory of tesseral-harmonics perturbations, resulting from the coupling between tesseral harmonics and J_2. These new formulations are being implemented in the precision orbit-computation program.

Because the accuracy of the inclination function in the precision orbit-computation program decreases for the higher geopotential orders, a new inclination function has been derived from group theory. Comparison of the two reveals that the new function is indeed more accurate for the higher geopotential orders. Furthermore, test results show that the new inclination function completely agrees with one derived by Gaposchkin, also from group theory. This new function has been implemented into the precision orbit-computation program.

Also during this reporting period, Ms. Barbara Romanowicz's (1975) Special Report dealing with resonance problems in artificial-satellite theory was published. Described more fully in Semiannual Progress Report No. 31, this paper discusses the use of the Lie-Hori perturbation method, with the objective of deriving a suitable algorithm valid for both deep and shallow resonance.

3.9.2 Radiation-pressure perturbations

Dr. Donald A. Lautman's work on the variable-albedo perturbation theory has been completed. In this theory, the earth's albedo has a latitudinal dependence given by $a = a_0 + a_z \sin^2 \phi$. We had previously discovered that a number of terms in the nonterminator expressions had to be expressed in infinite series. This difficulty has been overcome by means of a simplification that eliminates the factor $\csc^2\psi$, where ψ is the geocentric angle between the sun and the satellite, and allows the components of the disturbing acceleration to be expressed in the form of a finite Poisson series. Expressions for the perturbations of all the elements except the mean anomaly are given in closed form; those for the mean anomaly are open with respect to the eccentricity. An average of about 30 periodic terms appears in the expressions for the perturbations of the elements. The nonterminator expressions have been incorporated into the precision orbit-computation program.

The terminator expressions are complete, but they have not yet been added to the orbit-computation program. Their length requires a more compact Fortran output routine from the computer algebra program. The terminator expressions are not in closed form since, as in the case of the uniform albedo theory, they require the expansion of $\sin \psi$ and $\pi - \psi$. In addition, the variable-albedo expressions necessitate the expansion of $1/\sin \psi$. However, since the terminator expressions are used only in the vicinity of $\psi = 90°$ and $270°$, the singularity is avoided and a straightforward expansion in terms of the argument of the latitude is possible. There are of the order of 100 periodic terms in the perturbation of each element.

The variable-albedo theory has been tested in the orbit-computation program by plotting the results of the theory against the numerical-integration method. Another version of the program, incorporating Lautman's latest albedo and infrared-radiation theories, is being tested.

Testing is also being done on a version of the program to compute radiation-pressure perturbations in which the albedo value can be altered or the radiation values not used.

Analytical expressions for the delayed infrared radiation-pressure perturbations on an earth satellite have been completed and are being implemented in the precision orbit-computation program. The infrared emissivity of the earth is assumed to have a latitudinal dependence given by $E_{ir} = b_0 + b_2 \sin^2 \phi$, where $b_0 \simeq 0.380$ cal cm^{-2} min^{-1} and $b_2 \simeq -0.117$ cal cm^{-2} min All the elements exhibit long-period perturbations of frequency $2\dot{\omega}$, while the elements ω, Ω, and M have secular perturbations as well. Since the nonradial component of the perturbing force is in the meridional direction pointed away from the equator, the motion of the node is direct. The value of sin $\dot{\omega}$ depends on both $a(1 - e^2)$ and inclination, and it may be either positive or negative. The value of M is negative, owing to a slight decrease in the effective value of μ. The magnitude of the infrared perturbations is about 25% of the albedo effect. This study is now complete; it improves our understanding of the modeling of this nonconservative force and its effect on satellite motion.

Aksnes has continued refining his direct radiation-pressure theory through a study of the sun's motions and a satellite's perigee and node during one revolution. For the balloon satellite Dash 2 ($A/m = 42$ cm^2 g^{-1}), Table 16 shows the discrepancies between the theory and numerical integration after 200 days of motion. Figures are given in absolute measure and as a percentage of the total perturbation, respectively.

Table 16. Discrepancy between theory and numerical integration for Dash 2 for 200 days of motion.

Units	Δa	Δe	ΔM	Δi	$\Delta \omega$	$\Delta \Omega$
Absolute measure	18 m	-2.78×10^{-7}	-0.°88	$1.°02 \times 10^{-4}$	$-2.°03 \times 10^{-4}$	$4.°25 \times 10^{-3}$
Percent of total perturbations	0.67	0.001	0.96	0.16	0.01	1.3

During testing and application of Aksnes' radiation-pressure theory with actual observations, he discovered that the accuracy of his theory (particularly for the semimajor axis) could be substantially improved through a more accurate evaluation of the points of intersection (E_1 and E_2) between a satellite's orbit and the earth's shadow.

An apparent problem arose with the radiation-pressure computations for a particular arc of Pageos data, wherein the iterative method used to calculate the shadow boundaries E_1 and E_2 failed to converge. Aksnes checked the analytic computations through comparisons with numerical integrations. Although a slight inaccuracy had been introduced in the theory, because of the slow convergence of the iterative calculation when the points of entry into and exit from the earth's shadow lie close together, the problem appeared to be connected with the albedo part rather than with the direct part of the radiation-pressure perturbations. A more reliable and more efficient algorithm has been derived and programed for computing the shadow-crossing points of earth satellites. The new algorithm also works in situations where the old one failed because of lack of convergence.

3.9.3 Reference systems

An analytical theory for the motions of the three planes normal to the angular-momentum axis, normal to the figure axis, and normal to the rotational axis of the triaxial rigid earth has been completed by Kinoshita. The present theory utilizes Andoyer's variables, a moving reference plane, and Hori's (1966) perturbation averaging method.

A comparison with Woolard's (1953) theory shows that 1) the maximum difference in nutation for the plane normal to the angular-momentum axis and calculated from the same constants used by Woolard is 0".0017, 2) the discrepancy in Oppolzer terms is larger than the discrepancy in nutation for the plane normal to the angular-momentum axis, and 3) the present theory does not include secular terms, which in Woolard's theory have an effect on the establishment of the reference system. Coefficients as large as 0".0001 in nutation

for the three planes have been calculated by employing the numerical values recommended at the working meeting of the International Astronomical Union held in Washington during September 1974.

The updated nutation terms, previously obtained and verified by Kinoshita, have been incorporated into the precision orbit-computation program.

Published during this period was Kinoshita's (1975) Special Report, in which literal expressions are constructed for the precessional motion of the mean equator referred to an arbitrary epoch.

3.9.4 Field computing capability

The minicomputer systems at Mt. Hopkins and in Brazil, Peru, and South Africa are now operating in a stand-alone mode, receiving satellite orbital elements and generating laser-satellite pointing predictions for subsequent use by the laser mount system.

The new version of the prediction software for this mode includes the ability to read elements from Cambridge and to handle extended radio fadeouts. Also incorporated are a superior mount-correction program; diagnostics for power failure of Linc tapes, in Fortran; and improvements to the Forth power-fail code.

Minor modifications have been made to existing programs so that gravity-field data on new satellites can be transmitted to the field in order to generate pointing angles. Other programs have been written to copy from Linc-tape to disk and from disk to magnetic tape. Software has been designed to copy observations and calibrations to Linc tape at the field stations. A program to be run on the Nova in Cambridge copies these Linc tapes to industry-compatible magnetic tape for input to the CDC 6400. Work on Linc-tape diagnostics has begun.

The minicomputer laser prediction system now supports the routine 8-pulse-per-minute laser operation. A number of changes were made to the system at Mt. Hopkins, including the display of punch-program output lines on the Lexiscope, the addition of a paper-tape duplication facility, and the printing of true range in the pass summary. Changes were also made to permit programs to be modified from Cambridge.

3.10 Solid-Earth Surface Measurements (RTOP 161-05-06)

Surface measurements of plate deformation will be valuable input to an Earthquake Hazard Assessment model; the definition of such is a principal objective of EODAP. Mohr and Girnius have reduced the geodimeter measurements of the 1974 Ethiopian rift survey and believe it to be the most far-reaching and precise of all five Ethiopian surveys. Refined corrections and improved elevation values have been applied to the 514 lines comprising the geodimeter network. From the 1974 survey, corrections have been made for water-vapor pressure and for heights, necessitated by the use of differing numbers of prisms. The accuracy with which single, continual measurements under the same conditions were made is approximately ± 3.4 mm for both short (0.5 to 4 km) and long (4 to 25 km) lines. For multiple geodimeter measurements taken under varying conditions, the accuracy is about ± 4.2 mm. Figure 19 pictures the entire geodimeter network.

Free-net adjustments and classical analytical methods have been applied to the central, Mirrga network, shown in Figure 20, for the surveyed years 1970, 1971, 1973, and 1974. Results reveal significant, regular, lateral movements along the young rift-floor faults. We plan to prepare a detailed 1:10,000 tectonic map of this region.

The process of free-net adjustments solves for a congruent part of the network, which can be used to determine displacement vectors of significantly

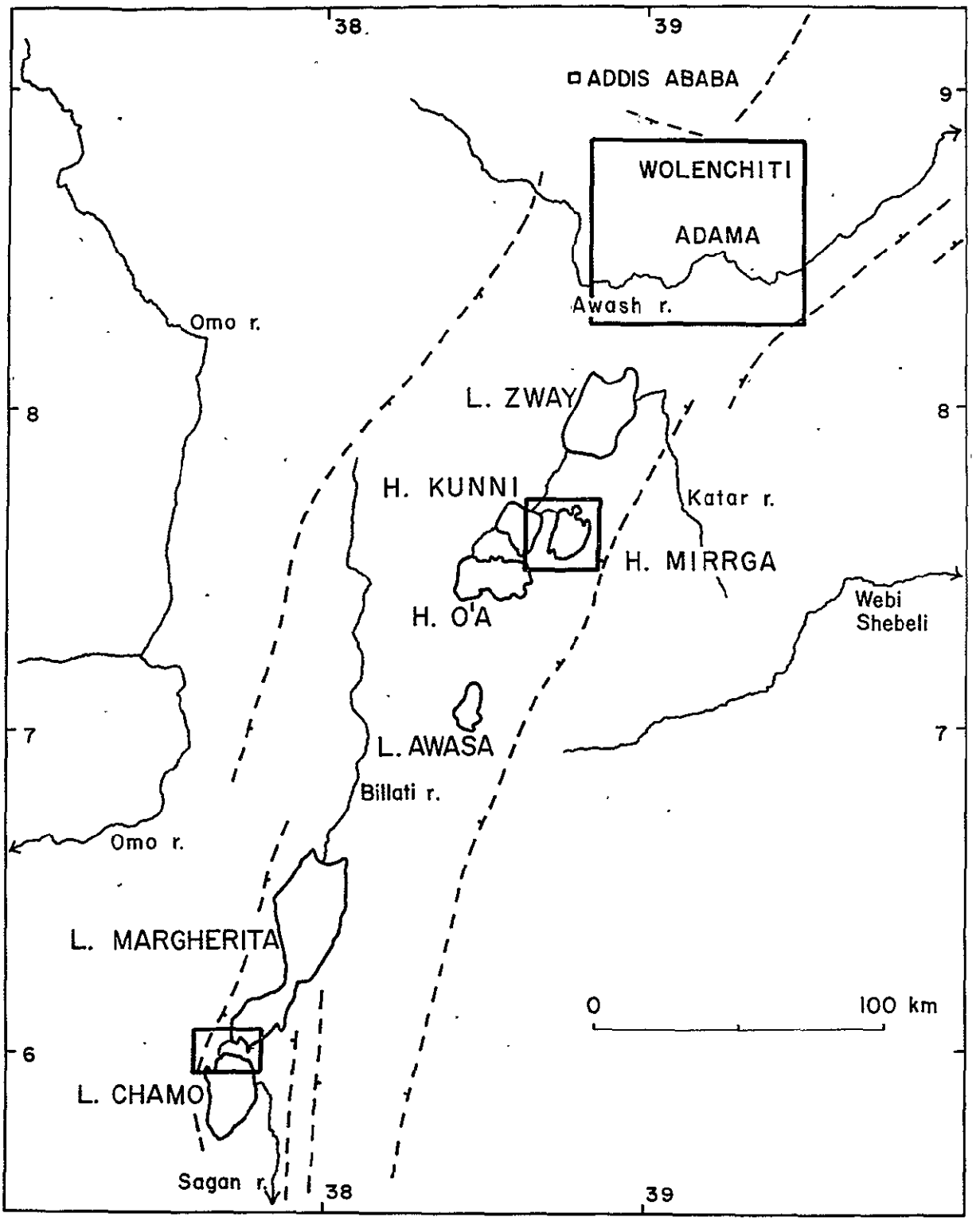

Figure 19. The Ethiopian rift (with boundaries indicated schematically), showing network sites.

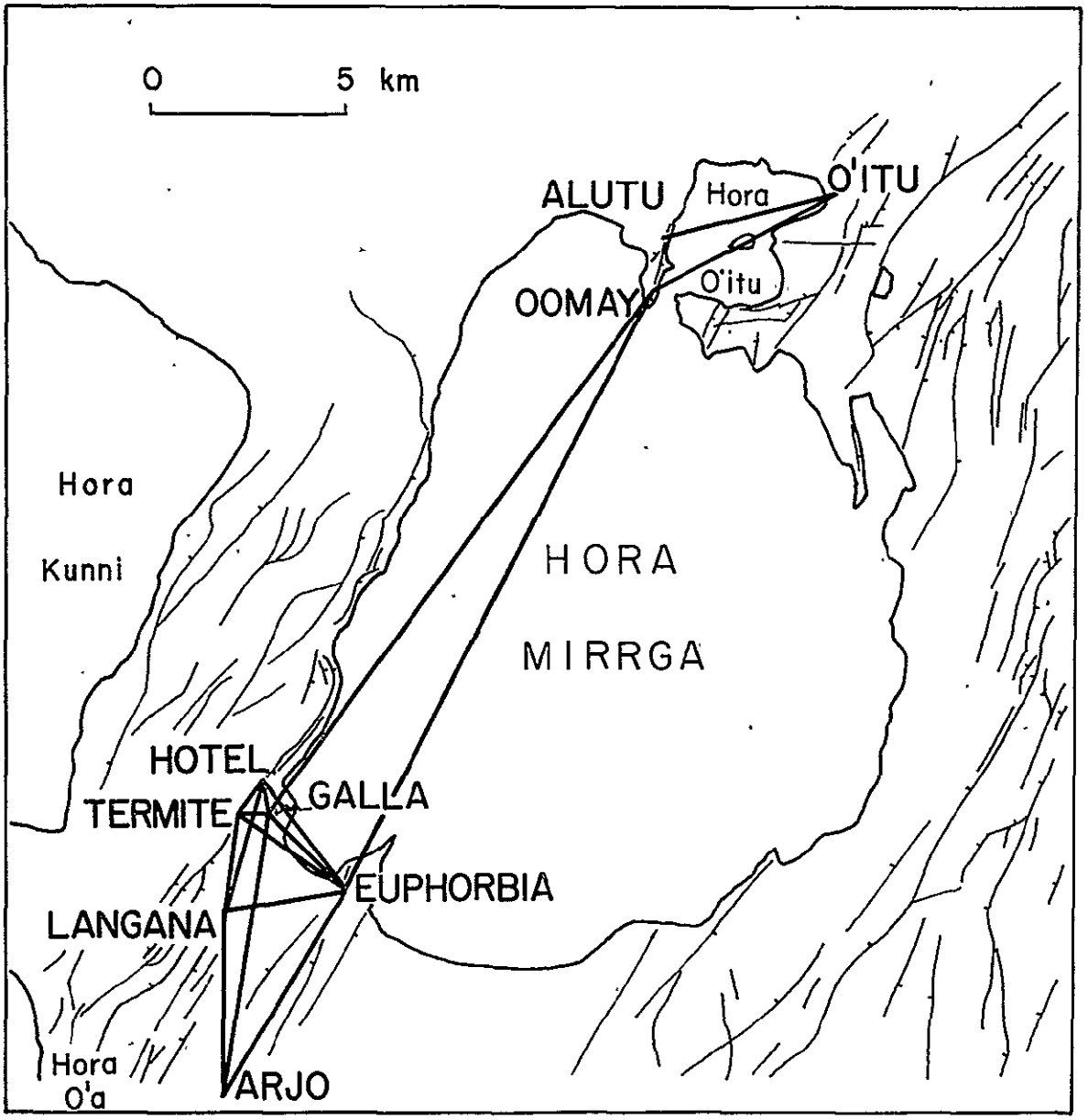

Figure 20. The Lake Mirrga network, showing preserved fault scarps.

active stations. The resulting sets of station coordinates for each respective year are then used to determine translation, rotation, and scale differences among the measurements made. Current results show that 1) changes from observed to computed line lengths are generally less than 1 part per million, and 2) computed errors of the lines are less than 3 mm. Because physical interpretation of free-net adjustment station vectors can be difficult in the absence of strongly obvious relative station motions, two stations lying on the same fault escarpment 1 km apart are now being used as a reference for analysis of other points.

Classical analysis of Wolenchiti, the northernmost network (see Figure 21), shows apparent extension rates that are greater than predicted by plate tectonics. This conforms with geological estimates from Ethiopia, and also with interesting new findings from Iceland, where crustal extension appears to be several times faster than on the mid-Atlantic ridge to the north and south. Although the cause of this peculiar behavior — hot spots? — is not yet understood, we hope that the Ethiopian geodimeter analysis will help resolve it.

With Dr. P. Einarsson of Lamont Observatory, Mohr planned an expedition to establish a trilateration network in south-central Iceland. The area, which includes the location of Iceland's largest earthquakes, is on the problematic southern transform zone, where P-wave velocity studies suggest that great strain is accumulating. Owing to the significant research that is likely to develop from such an expedition, the U.S. Geodynamics National Committee had selected this project to be part of their program on mid-Atlantic ridge studies. Unfortunately, though, insufficient funding has forced us to cancel the expedition.

Potassium-argon ages for volcanic rocks from the Eastern margin of the Ethiopian rift reveal major extension accompanied by dike intrusion and build-up of a 2000-m lava pile during the late Pliocene–early Pleistocene. This new evidence proves massive downwarping of the protorift trough. A minimum estimate of the rate of extension at the rift margin, derived from aggregate

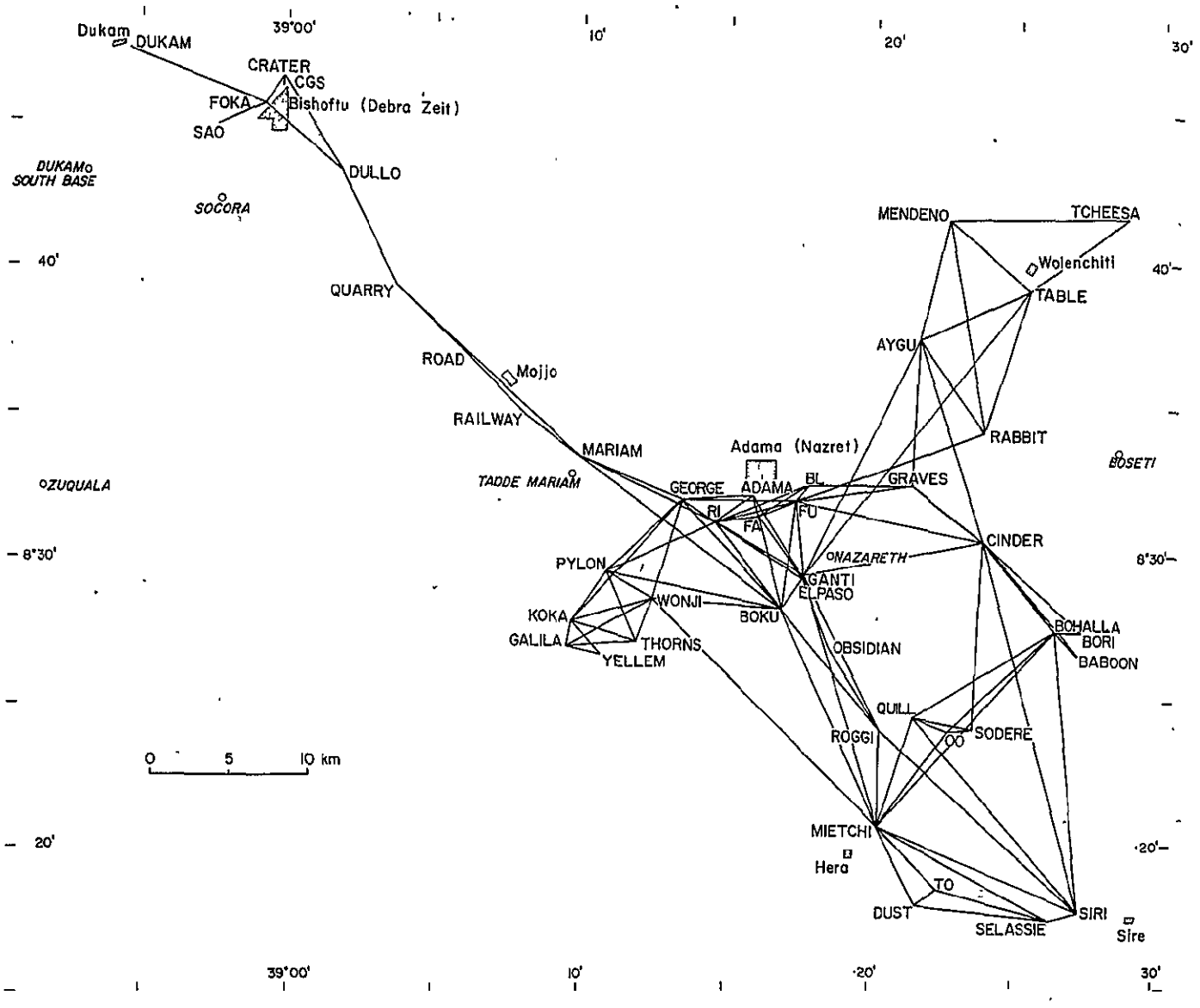

Figure 21. The 1973 Ethiopian geodimeter network at 8° to 9° N.

dike thickness and age range, is 0.25 mm $year^{-1}$, which conforms with plate-tectonic analysis of the Afar triple junction. Mohr (1975) presented these results at the American Geophysical Union meeting held in Washington during June.

An outgrowth of Mohr's studies is a proposed new classification of Ethiopian volcanic rocks, based on modifications of the Irvine and Baragar scheme. He has tested his scheme on 14 critically selected specimens against a background reexamination of the entire Ethiopian province. Mohr plans to submit this work to the 1976 International Geological Congress in an article entitled "A New Terminology for the Ethiopian Volcanics, with Special Reference to Transitional Basaltic and Intermediate Lavas and Dikes."

4. GEOS 3 PROJECT SUPPORT AND INTERNATIONAL COORDINATION

During this reporting period, SAO played an active role in providing support and international coordination for the Geos 3 project. This activity fell in two areas: 1) the laser tracking campaign, and 2) the coordination for international investigators.

4.1 Laser Tracking Campaign

In this area, SAO was to organize and manage the laser tracking participation of authorized overseas groups in support of Geos 3. This activity was intended to ensure that maximum effectiveness would be made of the available laser systems in carrying out the program objectives. The lasers are critical to this program because they have high ranging accuracy and they do not place any burden on the spacecraft power budget. Support from the overseas group is a very important part of the laser program, as their systems provide coverage in unique regions.

During this reporting period, SAO established operating interfaces and procedures with CNES for its lasers in Grasse (which later moved to San Fernando) and the Canary Islands and with the Institut für Angewandte Geodäsie for its laser in Wettzell. The arrangements were established in personal meetings and correspondence with both groups. SAO now furnishes them with orbital elements for predictions, schedules, and tracking priorities on a weekly basis. Each of the groups sends its quick-look data to SAO routinely, where they are incorporated into our weekly procedures to generate orbital elements for distribution. The data are screened at SAO, and reports on data evaluation and system diagnosis are fed back to the individual groups when appropriate.

SAO also provides these quick-look data to NASA/GSFC, NASA/Wallops, the National Oceanic and Atmospheric Administration, and NRL on a routine basis (by TWX), as requested by NASA.

SAO developed the software to provide quick-look data catalogs on a regular basis for project evaluation and investigator planning. These catalogs list all passes for which laser data were supplied on any satellite from any source (United States and overseas) and tabulate time and pass geometry for each case. The catalogs also contain monthly summaries.

During this period, SAO coordinated a preliminary doppler tracking campaign for the French and the West Germans. This campaign, on Geos 2, was undertaken to ensure that doppler tracking equipment would be ready by the launch of Geos 3.

4.2 Coordination for International Investigators

During the reporting period, we met with Geos 3 investigators from France, West Germany, Australia, and Israel to assist them in formulating their project requirements in terms specified by the Project Office. SAO reviewed all the proposals from the international investigators and furnished the Project Office with an assessment of feasibility and data and support requirements.

5. ATMOSPHERIC RESEARCH

The main activity in upper atmospheric research was concentrated on analyzing data from the ESRO 4 gas analyzer to determine a global model of geomagnetic effects on composition. The group also continued its analysis of drag data on a number of satellites, deriving atmospheric densities. These densities are the most comprehensive set of self-consistent data available and thus contribute significantly to an understanding of the earth's upper atmosphere.

5.1 Analysis of ESRO 4 Data

We received the final data from the ESRO 4 gas analyzer from Prof. U. von Zahn, of the University of Bonn, in January. These data supplement those Mr. Jack Slowey brought back last fall, and we now have approximately 400,000 independent composition records covering all latitudes under varying conditions during the satellite's 17-month lifetime. The entire data file has been converted to condensed binary form on 7-track tape and is available on either of two different sets of six tapes: a divided set of six individual tapes and a single, multireel file set.

Jacchia spent considerable time analyzing the ESRO 4 data with regard to changes in composition associated with geomagnetic disturbances. The primary tool was a program written by Slowey that determines residuals between the observations and an appropriate quiet model of the number densities of the different species at a particular height. These residuals are then plotted and studied to develop a model of the variations in composition associated with geomagnetically disturbed conditions. By comparing plots at different heights, the variations can be studied in different latitude regions simultaneously.

Number densities of four species (N_2, O, Ar, and He) have been measured at 9-sec intervals in the vicinity of perigee at heights between about 250 and

350 km. To expedite the analysis, we isolated those measurements that were made when the satellite was closest to heights of exactly 250, 260, ..., 310 km. For each of these heights, then, we had a pair of measurements, generally at widely different latitudes. The actual heights differ from the standard height by a few tenths of a kilometer, so the number densities were reduced to the exact standard height.

As a first step, we analyzed the 280-km data, with extremely interesting results concerning the behavior of the thermosphere during geomagnetically perturbed periods. The results of a paper presented on this topic can be summarized as follows (Jacchia, Slowey, and von Zahn, 1975):

A. During longer periods of sustained geomagnetic activity, the thermospheric temperature increases with geomagnetic latitude, reaching a maximum in the region of the magnetic pole. During short-lived magnetic storms, there is some indication that the maximum temperature may be reached at medium-high latitudes, probably in the auroral zones. A geomagnetic disturbance causes an increase of temperature in the thermosphere of $\Delta T \approx 82° K_p \sin^2 \phi'$, where K_p is the 3-hourly planetary geomagnetic index; ϕ' is the magnetic latitude computed from the adiabatic invariant, the so-called "invariant" latitude; and T is the exospheric temperature.

B. The observed variations of composition in middle and high latitudes can be explained by assuming that changes of temperature are accompanied by changes in height of the homopause. The reaction of the homopause to a change in temperature is not instantaneous, so dz_H/dT increases with time until an equilibrium value is reached. The value of dz_H/dT is about 30 m $°K^{-1}$ during short-lived storms, but may exceed 50 m $°K^{-1}$ during prolonged periods of high K_p; this difference shows that it takes some time (1 to 2 days) for the homopause to reach equilibrium conditions. The behavior of atomic oxygen is particularly sensitive to dz_H/dT: at 280 km, O varies in phase or in antiphase with respect to N_2 according to whether dz_H/dT is smaller or larger than 24 m $°K^{-1}$. The behavior of each atmospheric species can be neatly predicted from this model, without the introduction of any empirical factors.

C. At the geomagnetic equator, ΔT should be zero, and this is also in agreement with the observations, which show all four species varying in phase

with nearly equal amplitudes, following the K_p variations with a lag of about 8 hours (while the lag is minimal at high magnetic latitudes). Such behavior points to two density waves proceeding simultaneously from high latitudes, north and south, and meeting at the equator.

They are comparing these results with those from drag analyses on other satellites during the same period. The absolute accuracy of the ESRO 4 results will be important in the study of longer period effects later on. It may also be that the total densities can be used in connection with drag determinations on a satellite to study the drag coefficient and its variations with shape.

Jacchia and Slowey have also discussed with von Zahn the possibility of doing correlative studies between atmospheric variations and variations in extreme-ultraviolet (EUV) radiation using EUV data from ESRO 4.

5.2 Atmospheric Models

A global model of the geomagnetic disturbance based on the results just described has been worked out; the parameters are in the process of refinement. The model constructed last year, of the changes in composition during the diurnal variation, has proved satisfactory. Changes, however, were made in the model of the seasonal-latitudinal variations of temperature and composition, to account for more recent rocket and satellite mass-spectrometer data, which again point to a systematic change in the height of the turbopause with latitude and season. All the parameters of the models have been checked against the 50,000 density determinations from satellite drag that have been obtained from 1958 to 1975.

Jacchia has also devoted a little time to investigating the possibility of constructing a simple model of magnetic latitudes. Magnetic latitudes are more realistic than geomagnetic latitudes based on a centered dipole, but less complex than the "invariant" latitudes based on the integral invariant, which involves the use of an expansion of the earth's magnetic field in terms of spherical harmonics.

5.3 Determination of Densities through Drag Analysis

Jacchia and Slowey have continued analyzing drag data for six satellites in eccentric orbits with perigee heights between 250 and 750 km. Their atmospheric density determinations are now complete to the end of December 1974. The corpus of more than 50,000 densities provides a unique, uninterrupted monitoring of the atmosphere over a 17-year period, covering two maxima and two minima of solar activity. Duplicates of the tapes containing the material have been requested by several research institutions in, for example, France, Germany, and Hungary and are being used as an indispensable background for diverse investigations.

Work has been completed on a new catalog of densities from satellite-drag analysis. Included are results from the five balloon satellites 1961 δ1, 1963 53A, 1964 4A, 1964 76A, and 1968 66A. All the data from 1963 53A and 1964 76A and most of those from 1961 δ1 are based on precisely reduced Baker-Nunn observations. This is the first publication of such results, which have considerably better time resolution than those from field-reduced Baker-Nunn observations. For all five satellites, the reflection factor associated with the effect of radiation pressure has been more accurately determined than in the past. The effect of earth radiation pressure was also precisely included in every case. The densities are thus the most accurate available from the balloon satellites. They will be published as an SAO Special Report (Jacchia and Slowey, 1975).

5.4 Atmospheric Rotation

Slowey did some further work on the so-called "superrotation" (i.e., the net eastward motion) of the atmosphere. Primary interest was in the region above 300 km, where the observational data are sparse and not very reliable. Preliminary calculations to determine rotation rates from the secular rate of decrease of orbital inclination were carried out for six satellites, for which complete drag and orbital data are available. The possibility of using satellite data from other agencies was investigated; unfortunately, not a

single case was found where a reliable result could be expected that would add significantly to our knowledge of systematic winds at satellite heights. He intends, however, to continue pursuing this matter. Other satellite data available at SAO still have to be investigated with respect to this problem.

5.5 Publications

In addition to the publications referred to in the previous subsections, Slowey's paper on systematic winds determined from analyzing the orbits of balloon satellites and Jacchia's article on a search for lunar tides were published during this reporting period (Slowey, 1975; Jacchia, 1975). Both topics were discussed in Semiannual Report No. 31.

6. REFERENCES

BARAZANGI, M., and DORMAN, J.

1969. World seismicity maps compiled from ESSA Coast and Geodetic Survey epicenter data, 1961-1967. Bull. Seism. Soc. Amer., vol. 59, pp. 369-380.

GAPOSCHKIN, E. M., editor

1973. 1973 Smithsonian Standard Earth (III). Smithsonian Astrophys. Obs. Spec. Rep. No. 353, 388 pp.

HORI, G.

1966. Theory of general perturbations with unspecified canonical variables. Publ. Astron. Soc. Japan, vol. 18, pp. 287-296.

JACCHIA, L. G.

1975. A search for lunar tides in the thermosphere. Journ. Geophys. Res., vol. 80, pp. 1374-1375.

JACCHIA, L. G., and SLOWEY, J. W.

1975. A catalog of atmospheric densities from the drag on five balloon satellites. Smithsonian Astrophys. Obs. Spec. Rep., in press.

JACCHIA, L. G., SLOWEY, J. W., and VON ZAHN, U.

1975. Latitudinal changes of composition in the disturbed thermosphere from ESRO 4 measurements. Presented at the 17th International COSPAR Meeting, Varna, Bulgaria, June.

KAULA, W. M.

1966. Tests and combinations of satellite determinations of the gravity fields with gravimetry. Journ. Geophys. Res., vol. 71, pp. 5303-5314.

KINOSHITA, H.

1975. Formulas for precession. Smithsonian Astrophys. Obs. Spec. Rep. No. 364, 25 pp.

MATHER, R.

1970. The Australian geodetic datum in earth space. UNISURV Rep. No. 19, Univ. New South Wales, p. 80.

MINSTER, J. B., JORDAN, T. H., MOLNAR, P., and HAINES, E.
1974. Numerical modelling of instantaneous plate tectonics. Geophys. Journ. Roy. Astron. Soc., vol. 36, pp. 541-576.

MOHR, P. A.
1975. New data on the evolution of the Ethiopian rift. Presented at the 56th Annual Meeting of the American Geophysical Union, Washington, D.C., June; submitted to Bull. Geol. Soc. Amer.

PEARLMAN, M. R., LEHR, C. G., LANHAM, N. W., and WOHN, J.
1975. The Smithsonian satellite ranging system. In Laser Tracking Instrumentation, ed. by G. C. Weiffenbach and K. Hamel, Publ. Faculty of Nucl. Sci. and Phys. Engr., Tech. Univ. Prague.

ROMANOWICZ, B. A.
1975. On the tesseral-harmonics resonance problem in artificial-satellite theory. Smithsonian Astrophys. Obs. Spec. Rep. No: 365, 47 pp.

SLOWEY, J. W.
1975. Systematic winds at heights between 350 and 675 km from analysis of the orbits of four balloon satellites. Planet. Space Sci., vol. 23, pp. 879-886.

TALWANI, M., POPPE, H. R., and RABINOWITZ, P. D.
1972. Gravimetrically determined geoid in the western North Atlantic. In Sea Surface Topography from Space, vol. II, ed. by J. Apel, NOAA Tech. Rep. ERL 228 - AOML 7-2, pp. 23-1 to 23-33.

WILLIAMSON, M. R., and GAPOSCHKIN, E. M.
1975. The estimation of 550 km X 550 km mean gravity anomalies. Smithsonian Astrophys. Obs. Spec. Rep. No. 363, 20 pp.

WILLIAMSON, M. W., and KIRSCHNER, L.
1975. Geophysical data base. Smithsonian Astrophys. Obs., February.

WOOLARD, E. W.
1953. Theory of the rotation of the earth around its center of mass. Astron. Papers, vol. 15, part 1, 128 pp.